

A multimodel comparison of stratospheric ozone data assimilation based on an ensemble Kalman filter approach

T. Nakamura,^{1,2} H. Akiyoshi,¹ M. Deushi,³ K. Miyazaki,^{4,5} C. Kobayashi,³
K. Shibata,³ and T. Iwasaki⁶

Received 30 August 2012; revised 13 March 2013; accepted 15 March 2013; published 13 May 2013.

[1] For future development of a high-performance ozone analysis system, we investigated the impact of model performance on stratospheric ozone analysis by using four different models with a common data assimilation framework. For assimilation of ozone and meteorological field variables, we used a local ensemble transform Kalman filter with the CCSR/NIES chemistry-climate model (CCM), the MIROC3.2 CCM, the MRI CCM, and the CHASER chemical transport model. We examined the effects of model biases on forecast/analysis of ozone based on multimodel comparisons of assimilation results. We assimilated ozone profiles provided by Aura/Microwave Limb Sounder (MLS) and total ozone provided by the Ozone Monitoring Instrument (OMI)-Total Ozone Mapping Spectrometer (TOMS). For all models, meteorological fields obtained from a global reanalysis dataset (JMA Climate Data Assimilation System) were also assimilated to provide a common framework without any spatiotemporal dependence of data observation quality. Ozone profiles obtained from assimilation of MLS observations showed good agreement with independent ozonesonde observations, with a mean bias of less than 5% in the stratosphere. We found that model bias originating from ozone chemistry degraded the assimilation performance of not only ozone but also temperature in the stratosphere. Assimilation of OMI-TOMS total ozone data agreed with the independent SCIAMACHY total ozone with a bias of less than 3%. However, a model bias in the tropospheric ozone concentration deteriorated the stratospheric ozone analysis. Finally, the use of both stratospheric ozone profile data and total ozone data greatly improved the overall performance of the ozone analysis, regardless of the model biases.

Citation: Nakamura, T., H. Akiyoshi, M. Deushi, K. Miyazaki, C. Kobayashi, K. Shibata, and T. Iwasaki (2013), A multimodel comparison of stratospheric ozone data assimilation based on an ensemble Kalman filter approach, *J. Geophys. Res. Atmos.*, 118, 3848–3868, doi:10.1002/jgrd.50338.

1. Introduction

[2] Stratospheric ozone influences temperature and global circulation in the stratosphere through radiative heating. Understanding the important roles of stratospheric ozone has required an ozone monitoring program and the generation of global ozone distribution maps. Ozone concentrations derived from satellite observations are currently available and are used for such purposes. The spatial and temporal frequencies of those observations are higher than

those of ground-based observational data (e.g., radiosonde or lidar data). However, there are some coverage limitations. Nadir soundings (e.g., TOMS, Total Ozone Mapping Spectrometer) have high horizontal resolution but low vertical resolution. Limb soundings, such as the Aura/Microwave Limb Sounder (MLS), have high vertical resolution in the middle and upper stratosphere, but their resolution and accuracy are generally poor in the lower stratosphere and the troposphere. Chemistry-climate models (CCMs) are useful tools for understanding the global distribution of ozone. CCMs, which are numerical models that incorporate chemical processes into a general circulation model, have recently been developed for long-term projection of stratospheric ozone and temperature and for assessment of their influence on the troposphere [e.g., *SPARC CCMVal*, 2010]. Assimilation of stratospheric ozone data derived from satellite observations into a CCM is expected to improve stratospheric meteorological analysis, including atmospheric circulation and the distributions of ozone and stratospheric temperatures, through more informed modeling of radiation-chemistry-meteorology interactions. For example, *De Grandpré et al.* [2009] demonstrated that

¹National Institute for Environmental Studies, Tsukuba, Japan.

²National Institute of Polar Research, Tachikawa, Japan.

³Meteorological Research Institute, Tsukuba, Japan.

⁴Royal Netherlands Meteorological Institute, De Bilt, Netherlands.

⁵Japan Agency for Marine-Earth Science and Technology, Yokosuka, Japan.

⁶Tohoku University, Sendai, Japan.

Corresponding author: T. Nakamura, National Institute of Polar Research, Tachikawa, Japan. (nakamura.tetsu@ees.hokudai.ac.jp)

©2013. American Geophysical Union. All Rights Reserved.
2169-897X/13/10.1002/jgrd.50338

assimilation of ozone data improved stratospheric temperature forecasts through modeling of radiative feedback based on the ozone analyses. Assimilation of ozone data also improves estimates of wind fields, because ozone can be regarded as a tracer in the lower stratosphere, where the chemical lifetime of ozone is a few months or longer, and use of information derived from the covariance of tracers and winds improves circulation fields in CCMs [Semane et al., 2009; Milewski and Bourqui, 2011]. Assimilation of ozone data using global three-dimensional (3-D) chemistry transport models (CTMs) has facilitated production of the global distribution of 3-D ozone fields, which is used for operational and reanalysis models [Eskes et al., 2003; Onogi et al., 2007] and evaluation of the atmospheric transport of ozone in the upper troposphere and lower stratosphere (UTLS) [Clark et al., 2007]. Moreover, vertical profiles of ozone concentrations are important for the retrieval of temperature from radiance measured by instruments on satellites [McNally et al., 2006; McCarty et al., 2009]. Because changes of stratospheric winds and temperatures affect tropospheric meteorology even near the surface [Thompson et al., 2006; Son et al., 2010], assimilation of ozone data derived from satellite observations might improve forecasts of tropospheric weather.

[3] Three-/four-dimensional variational (3D-Var/4D-Var) data assimilation and Kalman filter (KF) systems [Kalman, 1960; Kalnay, 2003] have been developed for assimilation of meteorological and ozone data, and many studies have examined the assimilation of ozone data obtained by satellites. For example, *De Grandpré et al.* [2009] showed that ozone assimilation by the 3D-Var technique improved forecasts of stratospheric temperature. *Elbern et al.* [2010] developed a 4D-Var assimilation system for stratospheric chemical species and improved analyses and forecasts of ozone and associated chemical species. *Kiese wetter et al.* [2010] produced a 29 year ozone dataset for the period from 1979 to 2007 by using a simplified KF for satellite data assimilation. *Sekiyama et al.* [2011] constructed a total ozone assimilation system by applying a four-dimensional local ensemble transform Kalman filter (LETKF). The LETKF has recently been developed as one application of ensemble Kalman filters (EnKFs) [Hunt et al., 2007; Miyoshi and Yamane, 2007]. An EnKF manages the background error covariance obtained from ensemble members of the forecast model (i.e., flow-dependent forecast error covariance). The fact that the background error covariance sampled with a limited ensemble member often has an unrealistic correlation between points distant from each other causes sampling errors. In order to reduce such sampling errors, LETKF adopts a local patch corresponding to each grid point of the model. This gives an advantage of high efficiency for parallel calculations under the concept of EnKF. LETKF induces an ensemble transform matrix, which is used to transform the background ensemble matrix into the analysis ensemble matrix in the analysis step. This also helps to reduce computational costs. As mentioned above, EnKF and 4D-Var systems have been employed for various assimilation systems. *Kalnay et al.* [2007] has reported that the assimilation performances of EnKF and 4D-Var are comparable.

[4] The 3D-Var/4D-Var assimilation techniques require the use of adjoint models. As a result, whenever the forecast

model is updated, the adjoint model must also be updated. The use of 3D-Var/4D-Var assimilation in a CCM therefore entails some maintenance costs. For CCMs, which incorporate numerous chemical processes associated with stratospheric ozone, EnKF has an advantage because in contrast to 3D-Var/4D-Var techniques, it requires only the model outputs (ensemble after forecast model integration). Moreover, the same EnKF code can be used in different models, and the assimilation performance can be compared among the models. However, in the EnKF framework, the background error covariance is often underestimated because of model error and sampling error. To prevent underestimation, covariance inflation and localization techniques are required [Miyoshi and Yamane, 2007]. Moreover, although the EnKF technique has been found to be effective for atmospheric tracer data assimilation [Miyazaki, 2009; Liu et al., 2012], it is still unclear whether EnKF assimilation works for ozone in the upper stratosphere and mesosphere. At those altitudes, the fact that the simulated ozone concentration may converge rapidly to a chemical equilibrium state with a bias indicates that the assimilation may not reduce the bias of the model.

[5] Most theories of data assimilation have been constructed on the assumption that models include no systematic errors; that is, models are assumed to be perfect. In fact, however, model biases exist and affect assimilation results [Li et al., 2009b]. *Lin et al.* [2008], for example, reported that model bias was the primary cause of forecast errors in an EnKF assimilation system. *Geer et al.* [2006] used KF, 3D-Var, or 4D-Var assimilation system to compare ozone analyses (i.e., assimilated ozone fields) among models. They concluded that the model performances with respect to both transport and chemistry play an important role in the assimilation performance. Recently, *Miyazaki et al.* [2012a, 2012b] applied the LETKF technique to assimilation of tropospheric compositional data. They showed that high model performance is important, and certain skills are needed to prevent undersampling of the background error covariance in chemical data assimilation.

[6] Perfect-model Observing System Simulation Experiments (OSSEs) have been widely used to evaluate the impacts of assimilation by using artificial observations with known error characteristics [e.g., Lahoz et al., 2005; Milewski and Bourqui, 2011]. In contrast, when real data are being assimilated, model/observation error characteristics are not completely determined. Therefore, it is possible to evaluate how the assimilation performance is affected by the unknown model errors. This is useful for the verification and improvement of the assimilation system. In this study, to examine how model bias affects stratospheric ozone results, we performed assimilation experiments using the LETKF system with global stratospheric ozone data derived from satellite observations and meteorological fields from the global reanalysis dataset. In our system, use of the reanalysis data might make evaluation of the performance of the assimilation system difficult, because the error characteristics of reanalyses may be unknown. However, by using the reanalysis data, we were able to reduce the costs associated with development of the complex observation operator and management of the spatial representativeness of observations, which are required for the assimilation of real observations. The experiments

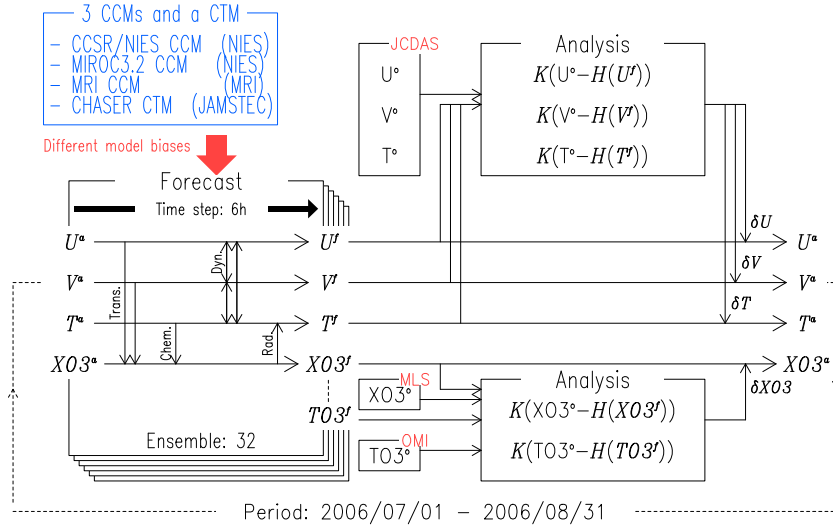


Figure 1. Schematic diagram of the assimilation system. The variables used for assimilation were zonal wind (U), meridional wind (V), temperature (T), ozone mixing ratio ($XO3$), and total ozone ($TO3$). Superscripts a, f, and o indicate analysis, forecast, and observation, respectively. K is the Kalman gain matrix, and H is the observation operator matrix. δ indicates analysis increment. Arrows indicate the flow of physical information. JCDAS, MLS, and OMI-TOMS are observation datasets.

involved four different chemical models developed independently by three institutes in Japan, and they were carried out for the same period of time and with almost the same parameters for the LETKF. Both the satellite observations and reanalysis dataset provided data that were almost uniform in time and space with respect to quality. This homogeneity facilitated the evaluation of model bias, which affects the assimilation results. Moreover, a comparison of the assimilation results among the models, whose model biases are different, allowed us to examine the influences of various model biases on the LETKF assimilation.

[7] Section 2 describes the models, the observational data, and the LETKF system. Section 3 describes the experimental setup for the LETKF assimilation. Section 4 provides the methodology for evaluation of the assimilation. Section 5 shows assimilation results for the meteorological fields, 3-D ozone profiles, and total ozone in general. Section 6 focuses on the intermodel comparisons and discusses how each model bias affects the assimilation performance. Finally, section 7 provides a summary.

2. Data Assimilation System

[8] The model variables used for assimilation (control variables) were zonal wind velocity (U), meridional wind velocity (V), temperature (T), and the ozone mixing ratio ($XO3$). The observation variables were U , V , T , $XO3$, and total ozone ($TO3$). First, in the forecast step (Figure 1, left), a 6 h forecast integration was performed for 32 ensemble members with different initial states. In the forecast step, U and V influence $XO3$ through ozone transport, and T influences $XO3$ through the temperature dependence of the chemical reactions, especially in the middle-to-upper stratosphere. Also, $XO3$ may have feedbacks to T through radiative heating and thus to U and V through the thermal wind balance. Hereafter, the variables with the superscript

f denote the forecasts (i.e., variables derived at the end of the model integration in the forecast step). Next, in the assimilation step (Figure 1, right), data assimilation was performed by LETKF by using the forecast error covariance estimated from the ensemble model forecast. The meteorological fields and the ozone fields were assimilated separately. In this analysis, we did not consider the cross-covariance (unless it is specified) between these fields to prevent errors in the model dynamics from influencing the ozone analysis (discussed in detail in section 3). The analysis is obtained by adding an analysis increment to the forecast (δx in Figure 1, where x indicates a corresponding variable). The new ensemble members obtained at one analysis step are used as the initial ensemble for the next forecast step. This assimilation cycle was repeated for the period from 1 July to 31 August 2006. We chose this period because the study was intended to be a first step for an assimilation study that used LETKF and global chemistry models. A purpose of the study was therefore to evaluate the global performance of ozone assimilation under typical stratospheric conditions during the summer in one hemisphere and winter in the other hemisphere. It would be interesting to examine the performance during the ozone hole season, when unusual chemical reactions cause severe destruction of ozone and bring unusual conditions to the stratosphere. Such a dramatic event would also be useful for examination of the performance of the assimilation and will be investigated in the future.

[9] We performed assimilation experiments with four forecast models and the same assimilation system. Next, we describe the models, observational data, and experimental settings.

2.1. Forecast Models

[10] We used three CCMs and one chemical transport model (CTM) (Table 1). SPARC CCMVal [2010] describes two of the CCMs (CCSR/NIES and MRI) and their outputs for CCMVal2 simulation.

Table 1. Model Resolutions, Transport Schemes, Modeled Chemistry, Inflation Parameters, and Initial Ensembles

	Resolution (Number of Vertical Layers in Troposphere/Stratosphere and Model Top)	Transport Scheme	Modeled Chemistry Region	Covariance Inflation	Initial Ensemble Members
CCSR/NIES CCM [Akiyoshi et al., 2009]	T42L34 (11/23) 0.01 hPa	Spectral advection	Stratosphere	Adaptive (1.0–2.0)	Output on 1 July in a free run over 32 years
MIROC3.2 CCM	T42L34 (11/23) 0.01 hPa	Semi-Lagrange	Stratosphere	Adaptive (1.0–2.0)	Output on 1 July in a free run over 32 years
MRI CCM [Shibata and Deushi, 2008; Deushi and Shibata, 2011]	T42L68 (14/54) 0.01 hPa	Semi-Lagrange	Troposphere and stratosphere	Adaptive (1.0–1.44)	Output at 00 UTC in a free run over 32 days (15 June through 16 July)
CHASER [Sudo et al., 2002a, 2002b]	T42L32 (15/17) 3.0 hPa	Semi-Lagrange	Troposphere	Fixed (1.21)	Randomly sampled with respect to local time on one day of a 32 day free run (15 June through 16 July)

2.1.1. CCSR/NIES CCM

[11] The Center for Climate System Research/National Institute for Environmental Studies (CCSR/NIES) developed the CCSR/NIES CCM [Akiyoshi et al., 2009], which has a T42 horizontal resolution and 34 vertical layers from the surface to 0.01 hPa, with about 3 km vertical resolution in the stratosphere. The CCM includes a detailed stratospheric chemistry module that incorporates interactions among chemistry, radiation, and dynamics (transport). The chemistry scheme for the stratosphere is also used in the troposphere. The scheme includes the oxidation processes of methane but does not include chemical reactions for nonmethane hydrocarbons and emissions of NO_x and CO. The lack of these chemical reactions and emissions may lead to an underestimation of ozone amount in the troposphere. This CCM has positive XO₃ biases in the upper stratosphere (10 to 2 hPa), possibly because of insufficient ozone destruction by the HO_x catalytic cycle, which in turn reflects the underestimation of water vapor in the stratosphere caused by a cold bias near the tropical tropopause [SPARC CCMVal, 2010; Eyring et al., 2006; Akiyoshi et al., 2009; Gettelman et al., 2010]. The positive XO₃ bias in this CCM causes a warm bias as a result of excessive solar heating by ozone in the upper stratosphere.

2.1.2. MIROC3.2 CCM

[12] NIES also developed the MIROC3.2 CCM, which has a T42 horizontal resolution and 34 vertical layers from the surface to 0.01 hPa, with about 3 km vertical resolution in the stratosphere. In this new version of the CCSR/NIES CCM, the dynamics and radiation components have been improved, but the chemistry module is unchanged. The major updates are as follows: the radiation scheme was updated by increasing the number of spectral bins (from 18 to 32), a semi-Lagrange scheme was adopted for the tracer transport, and a hybrid (sigma pressure) vertical coordinate system was adopted. These updates improved the cold bias at the tropical tropopause (i.e., the region of the cold trap), which was a problem of the CCSR/NIES CCM. The reduction of the cold bias caused an increase of water vapor in the stratosphere and thus a reduction of the positive XO₃ bias.

2.1.3. MRI CCM

[13] The Meteorological Research Institute (MRI) of the Japan Meteorological Agency (JMA) developed the MRI CCM [Shibata and Deushi, 2008; Deushi and Shibata,

2011], which has a T42 horizontal resolution and 68 vertical layers from the surface to 0.01 hPa, with about 1.5 km vertical resolution in the stratosphere. The vertical resolution of this model is about twice the resolution of the other two CCMs. Because the vertical localization distance is common among the models (section 2.3), the fact that the model has twice as many grid points as the other CCMs allows it to better acquire observational information. This might give the model the advantage of being able to obtain smooth analyses of the vertical distributions of both ozone profiles and meteorological fields. The chemistry module has been improved from the previous version described by SPARC CCMVal [2010] by incorporation of tropospheric chemical reactions and some new stratospheric chemical reactions (for details, see Deushi and Shibata [2011]). The MRI CCM has a cold bias in the Northern Hemisphere (NH) mid-stratosphere (upward of 30 hPa) and a negative XO₃ bias in the tropical upper stratosphere (20 to 5 hPa).

2.1.4. CHASER

[14] CHASER (CHemical AGCM for Study of atmospheric Environment and Radiative forcing) is a global CTM developed by Sudo et al. [2002a, 2002b]. It has a T42 horizontal resolution and 32 vertical layers from the surface to 3.0 hPa. CHASER has a detailed tropospheric chemistry module, but its upper boundary is in the middle stratosphere; thus, it cannot adequately represent the stratosphere. The meteorological fields (U , V , and T) in CHASER are nudged toward JMA Climate Data Assimilation System (JCDAS) data at all vertical levels. The six hourly data from JCDAS were linearly interpolated into the model grid. The relaxation time scale for nudging is 6 h. Above 70 hPa, XO₃ is nudged toward the climatology of ozone profiles obtained from MLS observations because of the lack of stratospheric chemistry. Below 70 hPa, XO₃ is calculated by the chemistry module, as in the three CCMs. Note that the climatologic ozone concentrations at levels above 70 hPa may affect XO₃ at levels near and below 70 hPa through transport. For example, the ensemble spread of ozone concentrations near 70 hPa becomes very small when an air mass is advected from the upper level by downward flow. Then XO₃ has a large effect on TO₃, because XO₃ in the lower stratosphere has a large impact on the TO₃ calculation. Thus, we did not perform assimilations of TO₃ in CHASER.

2.1.5. Intermodel Comparison Strategy

[15] Dependences of the assimilation performance of ozone concentration in the stratosphere on the model performance were examined by comparison of the assimilation results among the three CCMs. Because the meteorological fields were assimilated for all experiment of all models, most differences of the XO₃ analyses among models came from the model errors in the chemistry of the stratosphere. In contrast, differences of XO₃ analyses came from the transport in the UTLS region in *Geer et al.* [2006]. However, lack of tropospheric chemistry in CCSR/NIES and MIROC3.2 might cause some difficulties in detecting the influence of transport error. Therefore, CHASER CTM, which has the tropospheric chemistry module in the troposphere as well as MRI CCM, is useful for comparison with the three CCMs in the UTLS.

2.2. Observation Data

[16] Here we describe the observational data used in the assimilation experiments, giving detailed information on resolution, errors, and data screening methods.

2.2.1. Aura/MLS Ozone Profiles (XO₃)

[17] We used the MLS ozone profile dataset, version 2.2, as observational data for XO₃ [*Waters et al.*, 2006]. The ozone observations of the MLS cover the latitude range between 82°S and 82°N, with horizontal resolution between 160 and 300 km, and include the altitude range between 215 and 0.02 hPa, which is a suitable range for scientific purposes. The vertical resolution of the MLS is about 3 km in the stratosphere. The vertical resolutions of our models are the same or higher than the MLS resolution and thus are sufficient for effective assimilation of the MLS profiles. We used Level 2 (L2) XO₃ values and L2 precision as the observation errors. In our analyses, we applied the screening method used by *Froidevaux et al.* [2008] and *Livesey et al.* [2008] for validation of the MLS data. We did not apply averaging kernels to observation operators, because most values of the averaging kernel of the data are near unity. We used only the even-numbered data for “Status” fields, values larger than 1.2 for the “Quality” field, and values smaller than 1.8 for “Convergence” fields, an approach similar to the screening method of *Massart et al.* [2009]. This screening process removed data with a precision larger than the retrieval value. As a result, the errors of the screened data were never higher than 100% of the observation value (L2 value). Specifically, the errors were large near the upper (above 0.1 hPa) and lower (below 100 hPa) limits of the altitude range of the MLS observations. Averaged observation errors were less than 5% in most of the stratosphere.

[18] Version 3.3 of the dataset has been provided recently. In this version, the errors in ozone are improved and are at most 50% in the upper stratosphere. This version is also used for assimilation after data screening by the method described in the quality document (http://mls.jpl.nasa.gov/data/v3-3_data_quality_document.pdf) to evaluate the impact of observation errors on the analyses in the upper stratosphere (discussed in section 5.2.1).

2.2.2. OMI-TOMS Total Column Ozone (TO₃)

[19] We used the OMTO3G dataset version 3 provided by the Ozone Monitoring Instrument (OMI)-TOMS for total ozone data [*Bhartia et al.*, 2004; *Levelt et al.*, 2006]. These are gridded Level 2 data with a resolution of 0.25°. The data

have a time stamp indicating the observation time. As TO₃ observation data, we used the “ColumnAmountO3” values. OMTO3G data have a random error within 2%, depending on the solar zenith angle, aerosol amount, and cloud cover amount (see OMI Data User’s Guide, http://disc.sci.gsfc.nasa.gov/Aura/additional/documentation/README.OMI_DUG.pdf). In our analysis, we assumed an observation error of 2% for all OMTO3G data. In order to reduce differences of the spatial representativeness, the data were smoothed in a 2.0° grid to match the observation density of OMTO3G to the horizontal resolution of the MLS (160–300 km) and the models (around 2.8° ≈ 300 km at the equator). Data free from any systematic error were used for the smoothing (i.e., data with QualityFlag=0, which indicates, *inter alia*, a solar zenith angle less than 84°, no sulfur dioxide, and no glint contamination. See details in the user’s guide). Because the OMTO3G errors can be considered to be pseudorandom (see OMI Data User’s Guide), the observation errors were normalized by the number of pixels included in the smoothed grid. However, errors among neighboring pixels are not independent if, for instance, the surface conditions used in the retrieval are the same. Therefore, the observation error of total ozone in each 2.0° grid, estimated as between 0.1% and 2.0%, might be underestimated. The 2.0° gridded data were further thinned in the zonal direction to a data interval between 300 and 450 km (about 4.0° at the equator) to reduce the difference in observation density between low and high latitudes. In this study, a column-averaging kernel (AK) was not used to calculate total ozone in the models. In this case, the data assimilation may suffer from smoothing errors and retrieval errors arising from the a priori information. To cope with this problem, a joint assimilation of the observations of the total ozone and ozone profiles has been adopted in some studies [e.g., *Massart et al.*, 2009; *Pajot et al.*, 2011]. However, some studies have shown that assimilations of total ozone have worked without use of an AK [e.g., *Sekiyama et al.*, 2011]. If the AK is nearly constant with height, not using it may not degrade the analysis.

2.2.3. JCDAS (*U*, *V*, and *T*)

[20] We used a reanalysis dataset for the assimilation of the meteorological fields. For the global assimilation system, the raw data obtained by measurements should be used. Our main purpose was to evaluate the global assimilation performance of stratospheric ozone under a typical stratospheric condition. Therefore, we used reanalysis data, which are not real observations but have a temporally and spatially homogeneous observation density. We used instant *U*, *V*, and *T* values at 6 h intervals from the JCDAS reanalysis data. Whereas the horizontal resolution of the standard JCDAS dataset is 1.25 × 1.25°, we thinned them to a resolution of 2.5 × 2.5°. Variables at pressures between 1000 and 1 hPa, with vertical resolutions of about 2 km, were used for the LETKF assimilations in the CCSR/NIES, MIROC3.2, and MRI CCMs, and those between 1000 and 3 hPa were used for the nudging assimilation in CHASER. Because observation errors of the reanalysis data are not provided, we assumed the observation errors to be as follows: we calculated standard deviations every 6 h among five reanalysis datasets (JCDAS [*Onogi et al.*, 2007], NCEP/NCAR [*Kalnay et al.*, 1996], NCEP/DOE [*Kanamitsu et al.*, 2002], ERA40 [*Uppala et al.*, 2005], and ERA interim

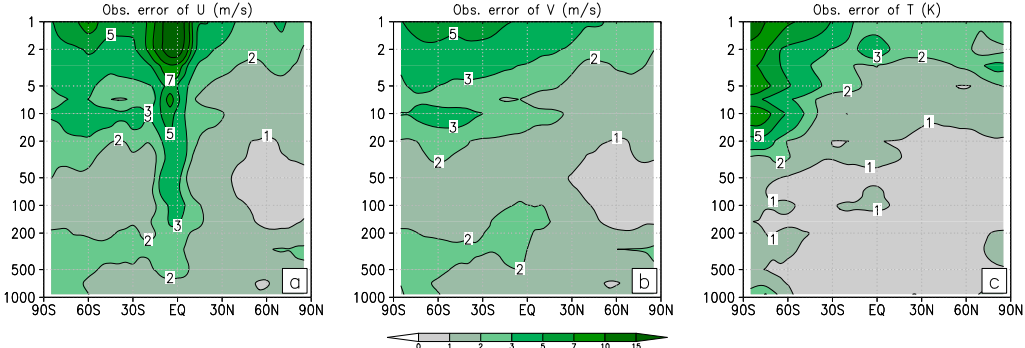


Figure 2. Zonal mean observation errors in JCDAS, based on the standard deviations among five reanalysis datasets (JCDAS, NCEP/NCAR, NCEP/DOE, ERA40, and ERA interim).

[Dee *et al.*, 2011]) and assumed that the monthly means of the standard deviations represented the observation errors. The standard deviations may reflect differences in the assimilated data, in the forecast models, and in the data assimilation schemes. Therefore, the JCDAS observation errors used in this study may differ from the observation errors of the actual meteorological observations. For instance, the zonally averaged observation errors for U were large in the tropical stratosphere (Figure 2), possibly because of differences among the reanalysis datasets originating from the quasi-biennial oscillation (QBO). The errors in T were large in the upper stratosphere (above 20 hPa) of the Southern Hemisphere (SH) and depended strongly on the model performance in each reanalysis, because there were relatively fewer observations in this region. These large errors in T may cause large errors in U and V in the SH upper stratosphere (above 10 hPa). In other regions, errors in U and V were less than 3.0 m/s, and those in T were less than 2.0 K. It should be noted that for reanalysis data, it can easily be supposed that the observation errors of different variables may be correlated. That is, it is better not to omit off-diagonal components in the observation error covariance matrix. However, in our system, we omitted them to reduce the computational costs.

2.3. LETKF System

[21] We used the same LETKF system to perform assimilation experiments with the four chemical models, but in fact, the LETKF parameters differed slightly among the assimilation systems of the four models.

[22] Previous studies reported that the ensemble size large enough to stabilize the LETKF is 20 for meteorological fields [Miyoshi and Yamane, 2007], 20 for total ozone [Sekiyama *et al.*, 2011], and 32 for tropospheric chemistry [Miyazaki *et al.*, 2012b]. In this study, the ensemble size of each model was set to 32. Because chemical forcing to ozone at a point is strongly affected by the ambient meteorological and chemical conditions around the point (e.g., temperature distribution), too large a localization distance is not suitable for an assimilation system that includes chemistry. Considering that the horizontal resolution of MLS observations and JCDAS is about 300 km, the horizontal localization distance was set to 650 km (a distance of about two grids of our models). The vertical localization distance was 0.4 in log-P units for the 3-D variables (XO3,

U , V , and T). We followed Sekiyama *et al.* [2011] by applying no vertical localization to 2-D variables such as TO3, and thus, the analysis increment obtained from the analysis error covariance matrix between TO3 and XO3 had the same weight at all levels. We used observational data within ± 3 h of each time step to update the control variables (XO3, U , V , and T ; see Figure 1) by LETKF assimilation every 6 h.

[23] The LETKF assimilation uses the forecast error covariance obtained from a finite number of ensemble members as the background error covariance. Many studies of meteorological assimilation have pointed out that the forecast error covariance obtained through the LETKF tends to be underestimated because of imperfections of the forecast model and the estimation error due to sampling error. Unusual growth of such underestimation errors is often referred to as filter divergence. Filter divergence may occur in our assimilation systems through the chemistry-dynamics coupling. For our ozone assimilation, the covariance underestimation may be serious in the upper stratosphere, mesosphere, and lower troposphere, where the chemical reactions are fast or emission sources of ozone precursors are close to each other. To counter this underestimation and to stabilize the assimilation, we needed to artificially inflate the magnitude of the forecast error covariance. Each of the four models used a different method for the inflation. The three CCMs used an adaptive inflation method [Li *et al.*, 2009a] that reduces the covariance underestimation caused by degeneration of the ensemble spread during a long-term assimilation. In some cases, however, the parameters used for adaptive inflation might be unrealistically large because they are estimated to be proportional to the difference between the forecast value and the observation. We therefore set an upper limit for the magnitude of the parameter. The upper limit was set to 2.0 in the CCSR/NIES and MIROC3.2 and to 1.44 in the MRI models. Then, for example, if the upper limit is 2.0, the inflated spread will never be higher than $\sqrt{2}$ times the spread obtained at the end of the forecast step. These limits were found to be adequate to prevent filter divergence in each model during the 2 months used for the assimilation. As a result, the covariance inflation parameter of the CCSR/NIES and MIROC3.2 CCMs varied between 1.0 and 2.0 (i.e., a spread inflation of 0–41%) and that of the MRI model varied between 1.0 and 1.44 (a spread inflation of 0–20%).

Table 2. Observation and Control Variables in the Four Experiments

Experiment	Observation Variables	Control Variables
O3-FREE	<i>U</i> , <i>V</i> , and <i>T</i>	<i>U</i> , <i>V</i> , and <i>T</i>
MLS	<i>U</i> , <i>V</i> , <i>T</i> , and XO ₃	<i>U</i> , <i>V</i> , <i>T</i> , and XO ₃
OMI	<i>U</i> , <i>V</i> , <i>T</i> , and TO ₃	<i>U</i> , <i>V</i> , <i>T</i> , and XO ₃
FULL	<i>U</i> , <i>V</i> , <i>T</i> , XO ₃ , and TO ₃	<i>U</i> , <i>V</i> , <i>T</i> , and XO ₃

CHASER used a fixed inflation parameter of 1.21 (i.e., a spread inflation of 10%). In CHASER, XO₃ is assimilated only below 70 hPa, where transport processes are much more dominant than chemical processes for ozone distribution, the result being that the degeneration of the spread due to chemistry may be negligible.

3. Experimental Design

[24] We designed and performed four experiments for multimodel evaluation of ozone assimilation (Table 2). In the O3-FREE experiment (EXP.O3-FREE), only the meteorological fields (*U*, *V*, and *T*) were assimilated. In the CCSR/NIES, MIROC3.2, and MRI models, the assimilation was done by LETKF, and in CHASER by nudging. In this experiment, the ozone concentration fields were calculated internally in each model by using the assimilated *U*, *V*, and *T* to calculate the transport and photochemical terms. In the MLS experiment (EXP.MLS), the 3-D ozone concentration fields (XO₃) of MLS were assimilated in addition to *U*, *V*, and *T*. In the OMI experiment (EXP.OMI), *U*, *V*, *T*, and total ozone fields (TO₃) provided by OMI-TOMS were assimilated. In the FULL experiment (EXP.FULL), *U*, *V*, *T*, XO₃, and TO₃ were assimilated.

[25] Milewski and Bourqui [2011] showed that the cross-covariance between ozone and dynamics is useful for improving both the ozone assimilation results and dynamics, but we have carried out experiments that took into consideration the cross-covariance. The results showed that the temperature bias increased because of the model bias in ozone (discussed in detail in section 6.2). Thus, this cross-covariance was not considered in this study and especially because of the large difference in the spatial distributions of the reanalysis data (meteorological data) and the satellite data (ozone). At each assimilation step, the coverage of the reanalysis data was global, whereas that of the satellite ozone data was not. Therefore, including the covariance would lead to a deterioration of the global ozone assimilation results because of the lack of ozone observations. Moreover, temperature and ozone are positively correlated with each other in the stratosphere. Therefore, even if model bias arises from only chemistry, the bias might affect estimates of both ozone concentrations and temperature. The result would be the addition of an unnecessary increment to the calculations at the analysis step. Actually, we have carried out experiments that took into consideration the cross-covariance. The results showed that the temperature bias increased because of the model bias in ozone (discussed in detail in section 6.2). Some assimilation systems based on a CCM use satellite radiance to reproduce temperature profiles. In this study, however, we used JCDAS for temperature observations.

[26] All experiments were performed for the period from 1 July to 31 August 2006. In the CCSR/NIES CCM, the data of the 32 initial ensemble members were obtained from a 32 year time-slice experiment under year 2000 conditions, the time-slice data having been taken from the outputs at 00 UTC on 1 July of the CCMVal-2 REF0 experiment [SPARC CCMVal, 2010]. In the MIROC3.2 CCM, the 32 initial ensemble members were obtained from a REF-0 - experiment using MIROC3.2 CCM, as was the case in the CCSR/NIES CCM. In the MRI CCM, the 32 initial ensemble members were obtained from a 32 day run from 15 June to 16 July by using the outputs at 00 UTC on each of the 32 days. In CHASER, the 32 initial ensemble members were obtained from a run from 15 June to 16 July by sampling the ozone fields randomly with respect to time. It is noteworthy that *U*, *V*, and *T* in CHASER were assimilated toward observations by a nudging technique. Therefore, their values were the same in all 32 ensemble members.

[27] The results for the first 15 days of the assimilation were not used in the evaluation of assimilation performance because the ensemble spread was not stable during this period. The results from 00 UTC on 16 July to 18 UTC on 31 August were used for the evaluation.

4. Evaluation of Assimilation Performances

[28] We evaluated assimilation performance by examining the bias, the root mean square error (RMSE), and the ensemble spread (SPRD), defined as follows:

$$bias = S[Hx - y^o]$$

$$RMSE = \left(S[(Hx - y^o)^2] \right)^{1/2},$$

$$SPRD = \left(SE[(Hx_m - H\bar{x})^2] \right)^{1/2},$$

where *x* is the 6 h forecast/analysis, *H* is the observation operator, *y^o* is the observation value, *m* is the ensemble member, and an overbar denotes the ensemble mean of forecast/analysis. *S[]* and *E[]* denote the spatiotemporal average and the ensemble average, respectively, and *SE[]* is an ensemble average of *S[]* or equivalently a spatiotemporal average of *E[]*. Bias and RMSE are the mean departure and standard error of the forecasts/analyses versus observations. Bias and RMSE are indicators of the accuracy of the forecasts/analyses, and SPRD is an indicator of their reliability. Bias and RMSE versus observations and SPRD were calculated at each time step of the assimilation. The RMSE should theoretically be comparable to the observation error if the LETKF assimilation works. For example, an abnormally large RMSE indicates a large model bias. In this study, we diagnosed the assimilation performance principally from the bias, RMSE, and SPRD of the forecast.

[29] We adopted two indicators as metrics of the growth rates of forecast/analysis errors (GRE) and ensemble spread (GRS) as follows:

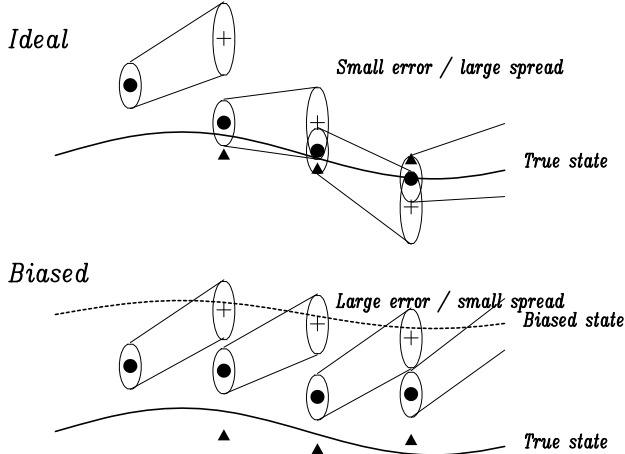


Figure 3. A schematic diagram of time flows in the LETKF assimilation system. Upper panel shows time flow in an ideal system. Bottom panel shows time flow in a biased system. Time flows from the left side to the right side of figure. Closed circle, cross, and triangle denote analysis, forecast, and observation, respectively. Ellipses encircling the symbols denote the corresponding ensemble spread. Thin solid lines connecting ellipses denote the growth of the spread in the forecast step. Thick solid and dashed (only in the bottom panel) lines denote the true and biased states, respectively.

$$GRE = \left(T \left[\frac{\left(RMSE_{t+1}^f \right)^2}{\left(RMSE_t^a \right)^2} \right] \right)^{1/2},$$

$$GRS = \left(T \left[\frac{\left(SPRD_{t+1}^f \right)^2}{\left(SPRD_t^a \right)^2} \right] \right)^{1/2},$$

where the superscripts f and a indicate forecast and analysis, respectively, and the subscript t indicates the time step of the assimilation. $T[\cdot]$ denotes the temporal average. A schematic diagram of the influence of the model bias on the growth of the errors and spread in the forecast step is summarized in Figure 3. In an ideal system (i.e., a model with no systematic bias), the analysis error and spread grow such that the ratio of their amplitudes in the forecast step is constant. Then in the analysis step, EnKF generates an analysis and spread optimized by taking the observations into account. Iterating this assimilation cycle brings the forecast/analysis close to the true state. In a biased system, however, all ensemble members approach the biased state without approaching the true state in the forecast step. Then the growth rate of errors becomes larger, and the growth rate of spread is reduced artificially in the forecast step. EnKF then underestimates the background error covariance in the analysis step, and thus, the analysis always has a bias that reflects the model bias. In CCMs, this uncorrected bias is caused primarily by the chemistry bias. We thus compared the GRE and GRS to elucidate the influence of the model bias.

[30] We evaluated the assimilation performance of XO3 and the meteorological field variables versus the MLS and JCDAS datasets, respectively. In principle, however, evaluation using a dataset that was used for the assimilation data is controversial. Therefore, we used two independent sets of observations, described below, to evaluate the assimilation of XO3 and TO3.

4.1. Ozonesonde Data

[31] We used ozonesonde data provided by the World Ozone and Ultraviolet Radiation Data Center (WOUDC, <http://www.woudc.org/>) as an independent dataset for the evaluation of XO3 assimilation. This dataset contains many observations made at NH mid-latitudes and fewer in other regions (Figure 4). Smit *et al.* [2007] have reported that uncertainties (random errors) of the ozonesonde measurements depend on the type of the ozonesonde. A systematic bias of ozonesonde data is not unusual. The data do not include information on observation errors. We thus followed Smit *et al.* [1998, 2007] and Geer *et al.* [2006] by assuming an observation error of 10% in the troposphere (below 100 hPa) and 5% in the stratosphere (at and above 100 hPa).

4.2. SCIAMACHY WFDOAS Total Ozone

[32] We used the gridded ($1^\circ \times 1.25^\circ$) total ozone data measured by the Scanning Imaging Absorption Spectrometer for Atmospheric Cartography (SCIAMACHY) (available at <http://www.iup.uni-bremen.de/gome/wfdoas/>) as an independent dataset to evaluate TO3 assimilation performance. SCIAMACHY provides daily global data except in the polar night region. We assumed an observation error of 3% globally for total ozone, as recommended by Bracher *et al.* [2005] in their validation study. As with the OMI-TOMS data, we did not use an averaging kernel of this dataset. It should be noted that OMI-TOMS, which we used for the data assimilation, has a slightly positive bias at global scale (up to 1% compared with ground-based observations) [Balis *et al.*, 2007; McPeters *et al.*, 2008], whereas SCIAMACHY, which we used for the validation, has a negative bias (up to 3% and 1% compared with satellite

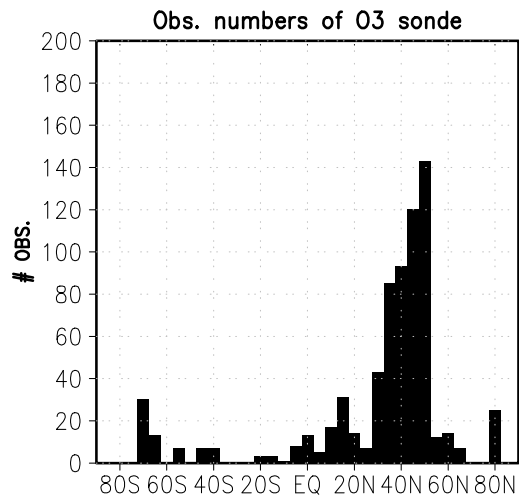


Figure 4. Observation frequency of ozonesonde data summed over the assimilation period (July and August 2006) in bins of 5° of latitude.

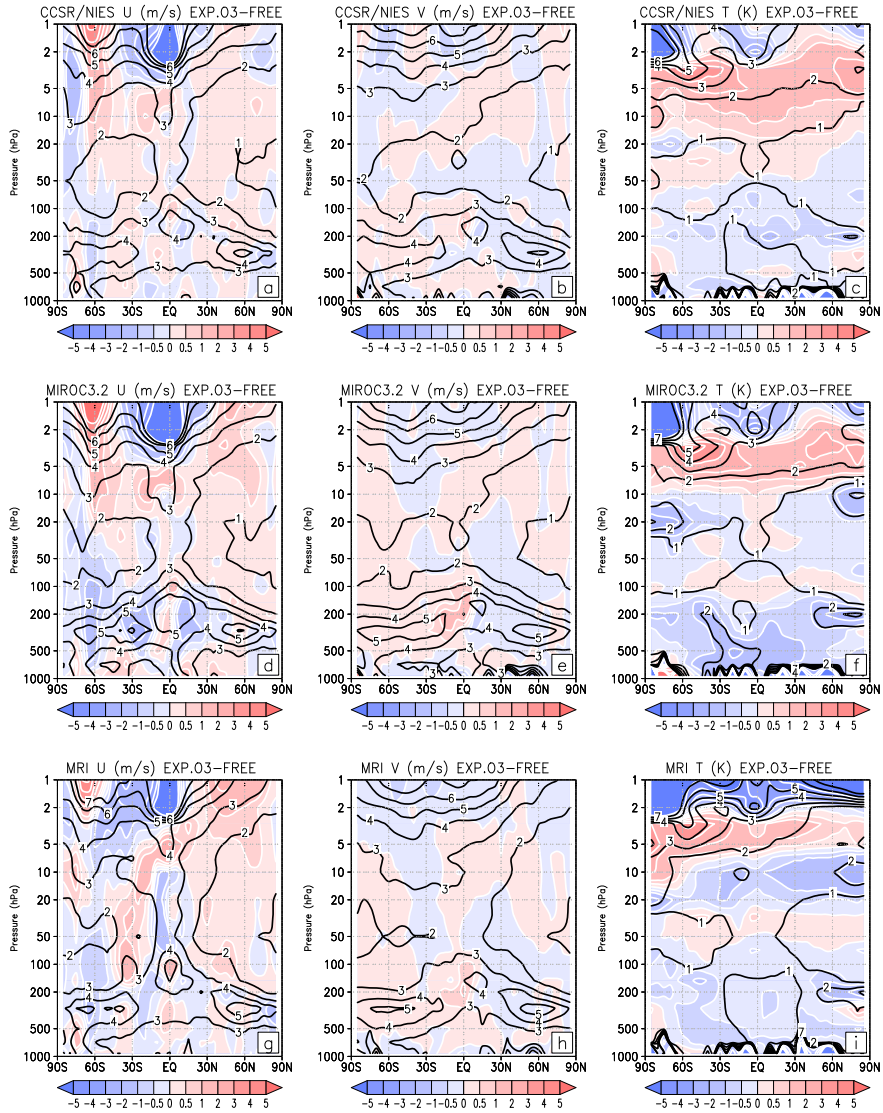


Figure 5. Zonal mean bias^f (color shading) and RMSE^f (contours) averaged for the period from 00 UTC on 16 July to 18 UTC on 31 August for U , V , and T in EXP.O3-FREE. (a–c) CCSR/NIES CCM, (d–f) MIROC3.2 CCM, and (g–i) MRI CCM.

and ground-based observations, respectively) [Hilsenrath *et al.*, 2004; Bracher *et al.*, 2007]. The influence of these biases should be taken into account when interpreting the results.

5. General Aspects of Assimilation Performances

5.1. Assimilation Performance of the Meteorological Fields

[33] We examined assimilation performances for the meteorological field variables (U , V , and T) in EXP.O3-FREE. The bias and RMSE shown in Figure 5 were computed against JCDAS itself. In the three CCMs, RMSEs of U and V , denoted by contours in Figure 5, are large in the upper stratosphere and near the tropopause and small in the lower and middle stratosphere (Figures 5a and 5b). The RMSE in T is almost constant up to the middle stratosphere and increases upward from there (Figure 5c). The fact that the RMSE structures of U , V , and T are similar to the JCDAS observation errors (Figure 2) indicates that the assimilations

worked properly. In the upper stratosphere, biases in U (denoted by color shading) are negative in the tropics and positive at high latitudes of the SH. The fact that a large positive bias of $T > 1$ K is commonly found near 5 hPa for all models might reflect bias of the JCDAS data. Onogi *et al.* [2007] have reported a considerable discontinuity in JCDAS temperature data that has resulted from a transition in the satellite data used for the assimilation (from TOVS to A-TOVS during 1998). After November 1998, JCDAS temperature data between 10 and 2 hPa show substantial negative anomalies compared to earlier data. In contrast, between 20 and 10 hPa, differences in the temperature bias among models are obvious. The CCSR/NIES data have a positive bias of about 1 K, MIROC3.2 data have less bias, and MRI data have a negative bias of about -2 K between 20 and 10 hPa. These differences among models in the temperature bias between 20 and 10 hPa imply a model bias associated with a radiative process that cannot be removed by assimilation of only the meteorological field. This issue will be discussed in section 6.2.

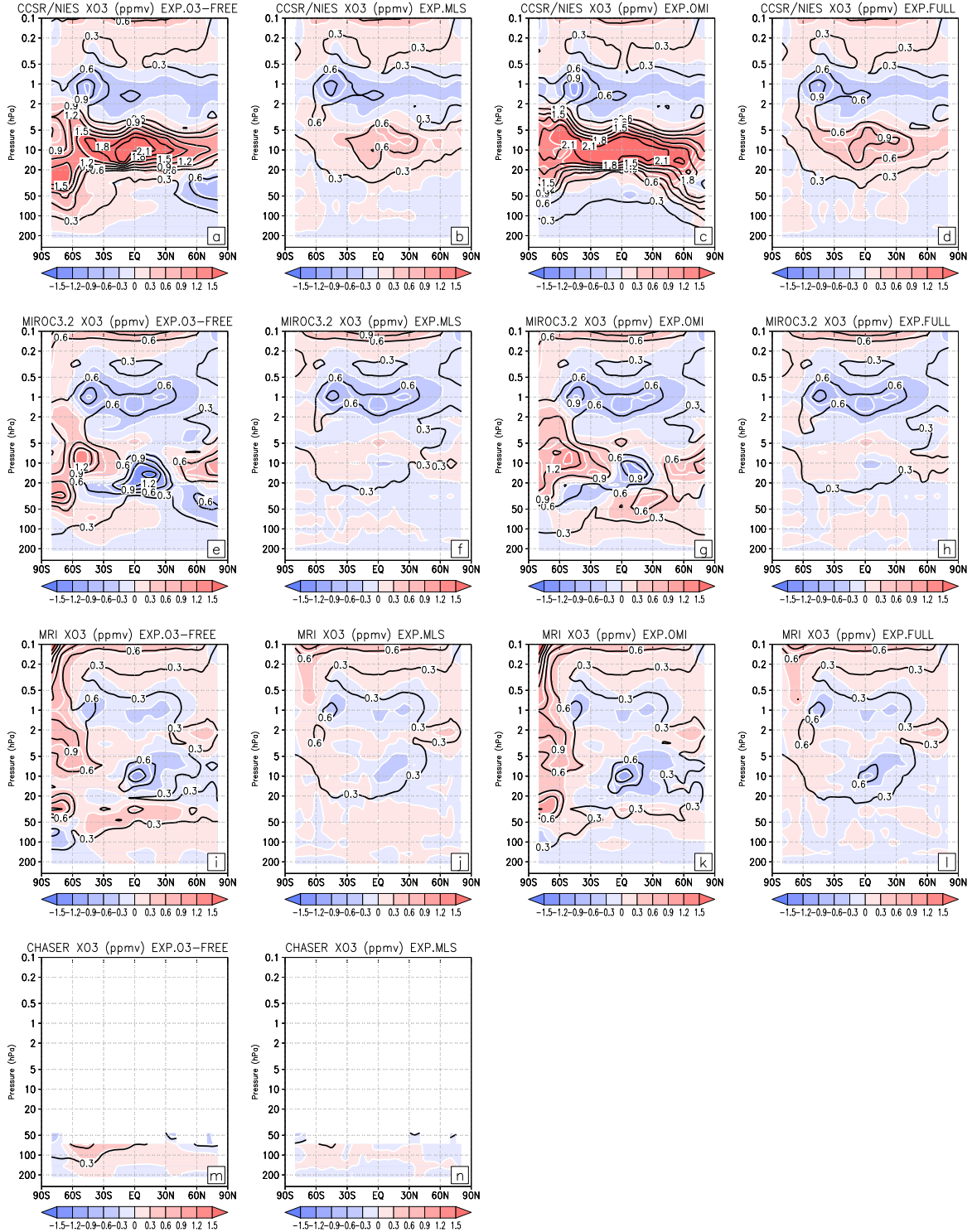


Figure 6. Zonal mean bias^f (color shading) and RMSE^f (contours) for XO3 averaged for the period from 00 UTC on 16 July to 18 UTC on 31 August in EXP.O3-FREE, EXP.MLS, EXP.OMI, and EXP.FULL. Bias and RMSE are calculated against the MLS ozone profiles. (a–d) CCSR/NIES CCM, (e–h) MIROC3.2 CCM, (i–l) MRI CCM, and (m–n) CHASER.

5.2. Assimilation Performance on the 3-D Ozone Profiles

[34] We next examined the assimilation performance for the 3-D ozone profiles by comparing the XO3 forecasts with the MLS observation.

5.2.1. In the Upper Stratosphere and Mesosphere

[35] Figure 6 shows the global distribution of the ozone bias^f and RMSE^f of each experiment and each model. In the upper stratosphere and the mesosphere, negative bias near 1 hPa and positive bias near 0.1 hPa are obvious and

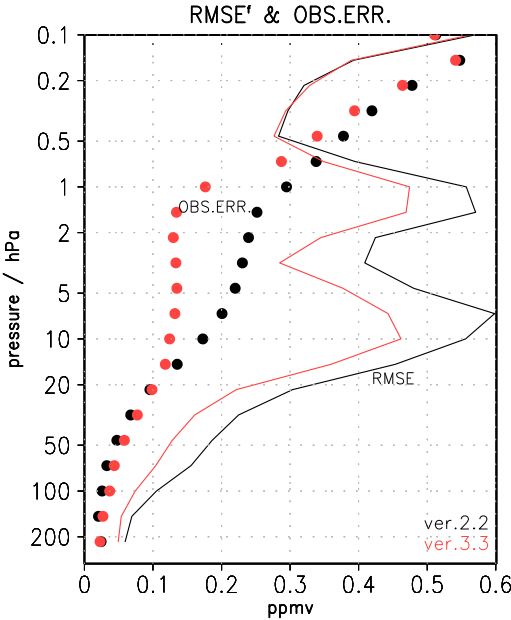


Figure 7. Vertical profiles of the global mean RMSE of XO_3^f in EXP.MLS of CCSR/NIES (solid lines) and observation errors in MLS ozone profiles (circles). Black, MLS version 2.2; red, MLS version 3.3.

common in the experiments with all of the CCMs (Figures 6a–6l). This result indicates that the MLS assimilation does not have enough of an impact in these regions. One reason for this inadequacy is the large magnitude of the observation errors in the MLS data in this region (Figure 7). In the MLS version 2.2, the errors begin to increase above 10 hPa and are large above 1 hPa. Therefore, we also examined assimilation by using the CCSR/NIES model and the newest version 3.3 of the MLS dataset, in which the observation errors in the upper stratosphere are 50% smaller than those in version 2.2. In EXP.MLS with version 3.3, the RMSEs in XO_3 in the stratosphere (from 200 to 1 hPa) were reduced by 10% to 30% compared to those in EXP.MLS with version 2.2. However, in the mesosphere (above 0.5 hPa), the RMSEs in XO_3 were not reduced in version 3.3. In the upper stratosphere and mesosphere, the ensemble spread of XO_3 rapidly converged within the forecast time step because the chemical lifetime of ozone (1 h or shorter) is shorter than the time step (6 h). For example, the fact that the global mean ensemble spreads of XO_3 in the CCMs above 5 hPa were smaller (around 0.1 ppmv) than the observation errors (0.2 to 0.7 ppmv) (Figure 8) implies a greater reliance of the LETKF on the model trial fields than on the observations, although the model error is large (0.3 to 0.6 ppmv of RMSE^f; Figure 7). This may result in a deterioration of the assimilation performance. Similar results were obtained by Geer *et al.* [2006], who concluded that the ozone photochemistry performance of the model is more important than the assimilation method for reproduction of the observed XO_3 distribution at these altitudes.

5.2.2. In the Middle Stratosphere

[36] In the middle stratosphere, the bias^f and RMSE^f of XO_3 in EXP.O3-FREE (Figures 6a, 6e, 6i, and 6m) were different among models, a reflection of the chemical model biases. The CCSR/NIES model had a positive bias greater

than 1.5 ppmv, with a large RMSE between 20 and 5 hPa; large RMSEs were also found in the lower stratospheric polar regions at 100 to 30 hPa, a reflection of the positive biases in the SH (up to 0.9 ppmv) and negative biases in the NH (around -0.6 ppmv). The MIROC3.2 model had a smaller bias and RMSE than the CCSR/NIES model, with the exception of the bias and RMSE in the lower stratospheric polar region, which were similar to those of the CCSR/NIES model. The MRI model had a smaller bias and RMSE, but in the lower stratosphere, a positive bias greater than 0.3 ppmv centered in the tropics at 50 hPa was evident. For CHASER, as described in section 2.1.4, the XO_3 above 70 hPa was nudged toward the MLS ozone climatology. Therefore, LETKF was used to assimilate the MLS ozone profiles only for levels below 70 hPa. A positive bias greater than 0.3 ppmv was evident in the SH lower stratosphere at 70–150 hPa. These biases were greatly improved by the assimilation of the MLS data (EXP.MLS; Figures 6b, 6f, 6j, and 6n). In most vertical levels of the stratosphere, RMSEs were reduced and were comparable to the observational errors of the MLS; the latter were nearly uniform horizontally and increased toward the upper atmosphere (Figure 8; 0.03, 0.2, and 0.3 ppmv at 100, 10, and 1 hPa, respectively). However, the RMSE near 10 hPa of the CCSR/NIES model remained large (around 0.6 ppmv) compared to other CCMs. This error probably reflects model bias. Although in general data assimilation techniques assume no model biases, LETKF reduced biases from over 1.5 ppmv to 0.6 ppmv and RMSEs from 2.1 ppmv to 0.6 ppmv. The RMSEs and biases in EXP.FULL (Figures 6d, 6h, and 6l) were similar to those in EXP.MLS.

[37] The assimilation of OMI-TOMS hardly reduced the biases and RMSEs in the stratosphere (EXP.OMI; Fig-

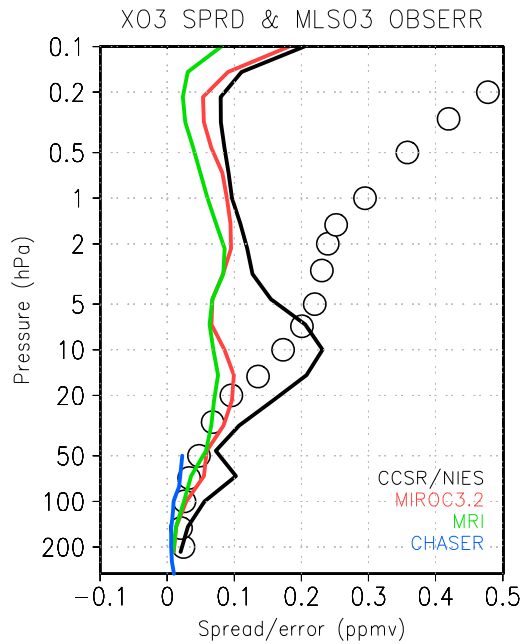


Figure 8. Vertical profiles of global mean observation errors in MLS ozone profiles (black circles) and ensemble spreads of XO_3^f in EXP.MLS in CCSR/NIES CCM (black line), MIROC3.2 CCM (red line), MRI CCM (green line), and CHASER (blue line).

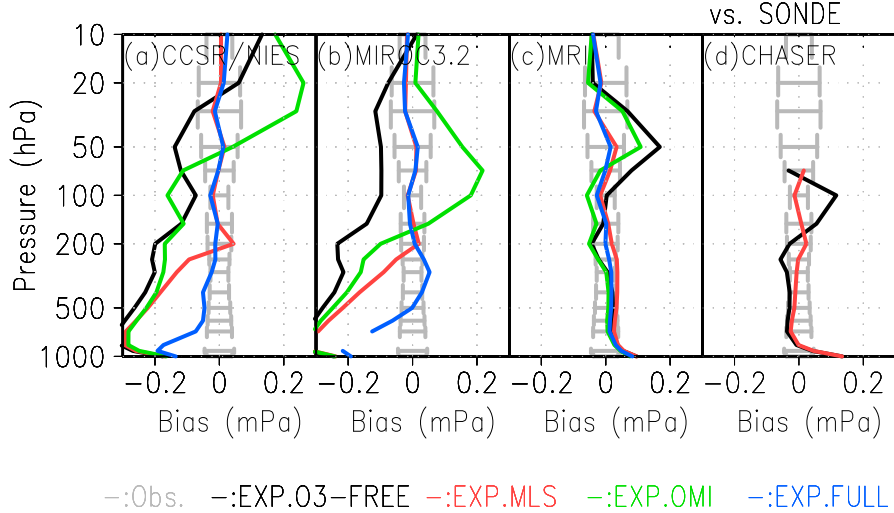


Figure 9. Biases in XO3^f averaged over NH (30°N to 90°N). The solid lines denote vertical profiles of the bias against the ozonesonde profile. The gray error bars are the observation errors. (a) CCSR/NIES CCM, (b) MIROC3.2, (c) MRI, and (d) CHASER.

ure 6c, 6g, and 6k). Figure 9 shows the XO3 biases against ozonesonde data averaged in NH. In some cases, biases were increased by the assimilation of OMI-TOMS compared to those without the assimilation. These cases are evident around 30 hPa in CCSR/NIES (green lines in Figure 9a) and around 70 hPa in MIROC3.2 (green lines in Figure 9b). In contrast, biases in the MRI model were reduced throughout the stratosphere by the assimilation of OMI-TOMS. As discussed in the next section, tropospheric bias was larger in the CCSR/NIES and MIROC3.2 models and was smaller in the MRI model, the implication being that bias in the tropospheric XO3 might affect XO3 analyses in the stratosphere. This possibility will be discussed in detail in section 6.4.

5.2.3. In the Upper Troposphere and Lower Stratosphere (UTLS)

[38] Figure 10 shows bias in the XO3 forecast of EXP.MLS at 100 hPa. In all models, biases were smaller than the MLS observation errors. This feature is commonly found at pressure levels between 200 and 70 hPa. However, below 300 hPa, where no observation was available, the model bias strongly affected XO3 profiles in CCSR/NIES and MIROC3.2 (red lines in Figures 9a and 9b). The MRI and CHASER models include tropospheric chemistry modules and thus have less bias in the troposphere. It is noteworthy that in CHASER, bias was reduced in the troposphere as well as in the lower stratosphere (red line in Figure 9d), even though the MLS observations included only a few vertical levels between 200 and 70 hPa that were used for assimilation. The improved vertical transport may be responsible for the good performance in the troposphere as well as the vertical covariance in XO3 does. Combined assimilation of MLS and OMI-TOMS (i.e., EXP.FULL) reduced the tropospheric biases in CCSR/NIES and MIROC3.2 (blue lines in Figures 9a and 9b).

5.3. Assimilation Performances on Total Ozone

[39] To evaluate the model bias in TO3 for each model, we constructed latitude-time Hovmöller diagrams of the zonal mean bias^f and RMSE^f in TO3 in EXP.O3-FREE

(Figure 11). Biases in TO3 were large during the evaluation period (16 July to 31 August), and the maximum value was more than 50 Dobson units, except in the MRI model. The TO3 biases in the models reflect the biases in XO3 below 50 hPa (Figures 6a, 6e, 6i, and 6m). TO3 biases showed a temporal drift, which resulted from the modification of the atmospheric transport field by the assimilation of the JCDAS data from 1 July. Differences in the latitudinal distributions of the temporal average of the zonal mean bias and RMSE were large among the models (Figures 12a and 12b). Assimilation of MLS ozone reduced the biases and RMSE in all models but did not eliminate them (Figures 12c and 12d). The temporal drifts of the bias in TO3 seen in EXP.O3-FREE were no longer seen in EXP.MLS (not shown). With the assimilation of OMI-TOMS total ozone (EXP.OMI), the biases in all of the models become smaller

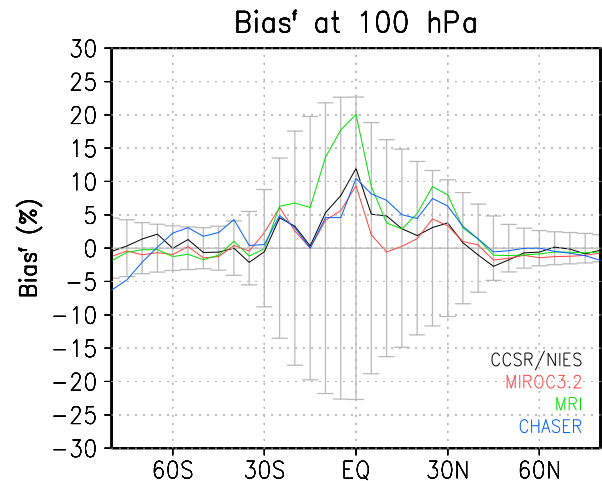


Figure 10. Zonal mean bias in XO3^f at 100 hPa averaged from 16 July to 31 August 2006. Models corresponding to the line colors are denoted at bottom right of the figure. Error bars denote the observation errors of MLS. The magnitudes are indicated by percentages (%) of the observation values of MLS.

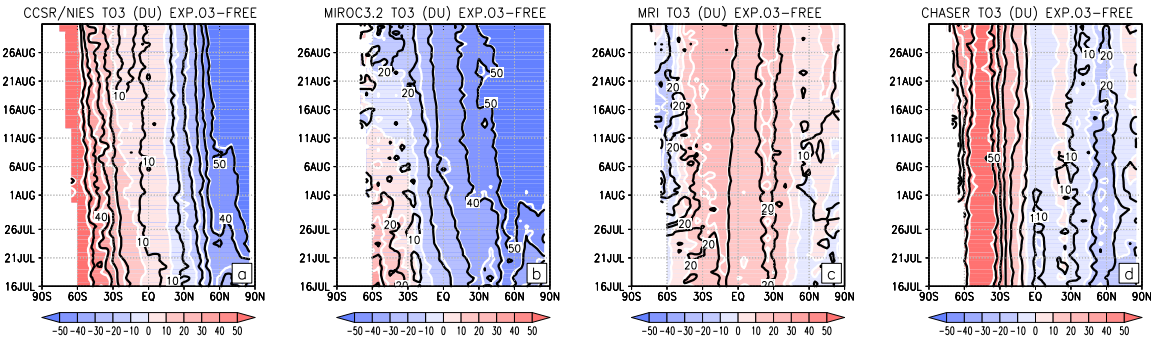


Figure 11. Zonal mean bias^f (color shading) and RMSE^f (contours) in TO3 in EXP.O3-FREE. Bias and RMSE are calculated against the SCIAMACHY total ozone. (a) CCSR/NIES CCM, (b) MIROC3.2 CCM, (c) MRI CCM, and (d) CHASER.

than the observation errors in SCIAMACHY (Figure 12e), but the RMSEs remained larger at high latitudes in the SH (Figure 12f). One of the reasons is that no OMI-TOMS observations are made in the polar night region. In the NH, only the RMSE in CCSR/NIES considerably exceeded the observation error. With the assimilation of both MLS and OMI-TOMS (i.e., EXP.FULL; Figures 12g and 12h), biases were smaller than the observation error, and RMSEs were comparable to the observation errors, except in the SH. Furthermore, the difference in the biases and RMSEs among the models was quite small. These comparisons indicate that the assimilation of only MLS data did not necessarily result in an excellent performance of assimilation for total ozone, whereas assimilation of both the MLS and OMI-TOMS datasets greatly reduced the influence of model bias on the assimilation performance.

6. Intermodel Comparison

6.1. Influence of Model Bias on Forecast/Analysis Error in Ozone

[40] As shown in subsections 5.1 and 5.2, the LETKF assimilation worked for both the meteorological fields and the MLS ozone profile in the CCSR/NIES, MIROC3.2, and MRI models. In particular, the positive bias in ozone near 10 hPa in the CCSR/NIES model was greatly reduced by the assimilation of MLS ozone profiles (Figures 6a and 6b). However, compared with the MIROC3.2 and MRI model results (Figures 6f and 6j), a relatively large bias still remained globally around this level in the CCSR/NIES model. The bias and RMSE of the XO3 forecast in the CCSR/NIES model were larger than those in the MIROC3.2 and MRI models near 10 hPa (Figures 13a and 13b solid lines). The SPRD^f in the CCSR/NIES model were also larger than the others (Figure 13c dashed lines). At this level, GRE (solid black line in Figure 13c) exceeded GRS (dashed black line) in the CCSR/NIES model, whereas in the MIROC3.2 and MRI models (red and green lines), GRE and GRS did not differ very much at all the pressure levels. This result indicates that in the CCSR/NIES model, the XO3 errors grew faster than the ensemble spread of XO3 in the forecast step. As a result, in the analysis step, the forecast error was underestimated, and the weight of the observation decreased. The LETKF then incorporated less observation information into the XO3 analyses.

6.2. Radiative Impacts of the Assimilation of XO3 on Temperature

[41] Because the temperature in the middle stratosphere strongly depends on the ozone concentration, a bias in XO3 may cause a bias in T . In the CCSR/NIES model, the bias^f in T at 10 hPa was reduced from around +1 K in EXP.O3-FREE to around 0 K in EXP.MLS, except in the polar regions (Figure 14a). The bias^f in XO3 was also reduced in EXP.MLS compared with that in EXP.O3-FREE (Figure 14b). Reductions of those biases were also obvious in the comparison against ozonesonde (Figure 14c). These results suggest that the assimilation of ozone data improves the modeled temperature through the radiative process of ozone heating. Figure 15a shows the global mean profile of radiative heating. Although near 10 hPa infrared diabatic heating (LW) is similar between EXP.O3-FREE and EXP.MLS, the fact that solar heating (SW) was 10% smaller in EXP.MLS than in EXP.O3-FREE led to a reduction of net heating (-0.3 K/day). Figure 16a shows evolutions of the bias in ozone concentration at 10 hPa in CCSR/NIES. The positive bias of 1.6 ppmv of EXP.O3-FREE was reduced toward a bias^a of 0.1 ppmv and bias^f of 0.4 ppmv by the MLS assimilation (EXP.MLS). The difference between bias^a and bias^f is due to the bias in the chemistry of the model, the result being that XO3 tends to return to the biased state in the forecast step as discussed in section 6.1. Figures 16b shows evolutions of the temperature bias at 10 hPa in the CCSR/NIES model. Bias of EXP.O3-FREE rapidly decreased 3 days after assimilation started (e.g., bias^a is +0.3 K). The biases gradually increased until 16 July and were steady after 16 July (bias^a is +0.9 K). This steady state was determined by the analysis increment, -0.18 K at every 6 h analysis cycle (difference between bias^a and bias^f), and the net radiative forcing, 0.7 K/day (Figure 15a). The steady state temperature was always lower than the radiative equilibrium temperature with the ozone bias (about 4 K at 10 hPa estimated from a free run of CCSR/NIES), and the 6 h assimilation cycle was shorter enough than the radiative relaxation time of temperature, 10 to 15 days at 10 hPa (about 30 km). Temperature therefore tended to be higher even in the 6 h forecast step. In EXP.MLS, net radiative heating decreased due to reduction of the ozone bias (0.4 K/day; Figure 15a). The steady state temperature then became lower (about +0.2 K). In contrast, in the MIROC3.2 model, positive bias in ozone was not responsible for the temperature bias (negative bias) (Figure 16c and 16d),

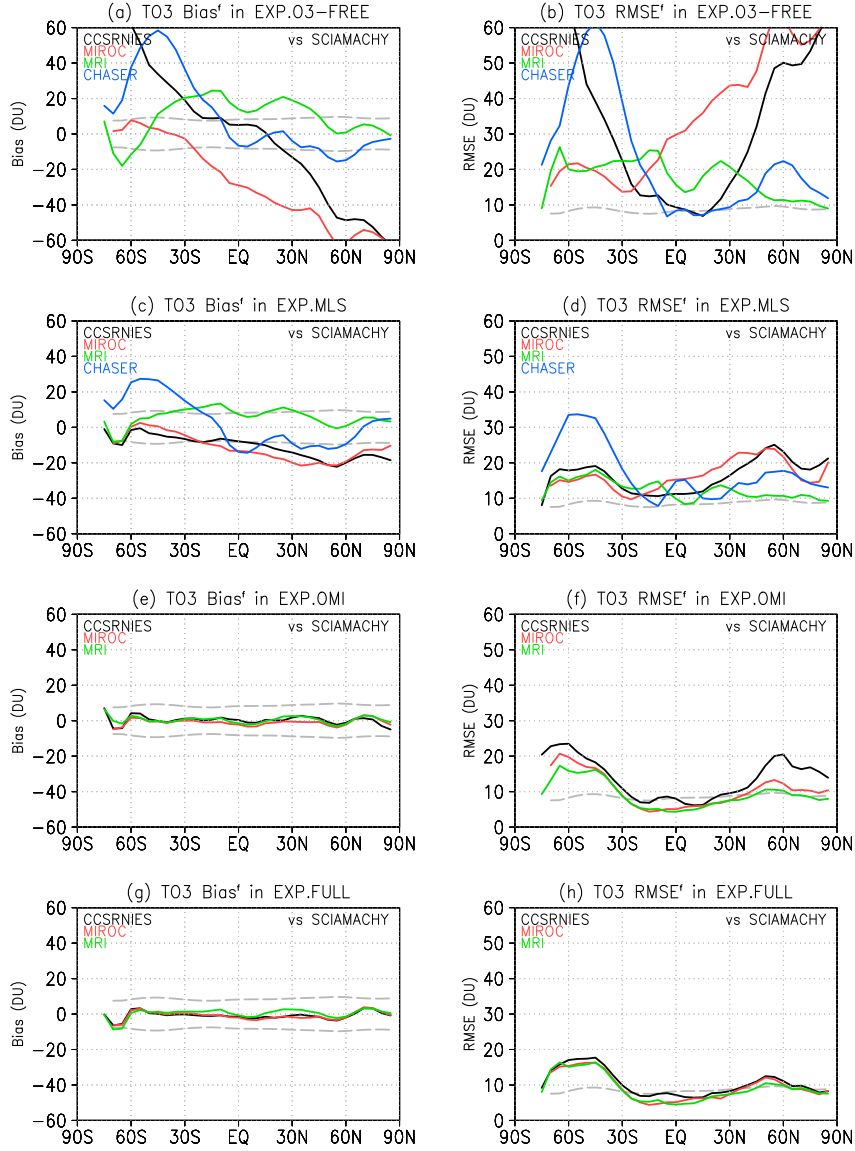


Figure 12. Temporal average of zonal mean (left) bias^f and (right) RMSE^f in TO3 against SCIAMACHY total ozone for the period 00 UTC 16 July to 18 UTC 31 August. Gray dashed lines denote observation errors. (a and b) EXP.O3-FREE, (c and d) EXP.MLS, (e and f) EXP.OMI, and (g and h) EXP.FULL.

implying that the radiation or dynamics may cause the model bias in temperature. The assimilation of the MLS therefore had less impact on the temperature analyses. We also confirmed that in the MRI model, the positive ozone bias and warm bias at 50 hPa were improved by the assimilation of the MLS ozone profiles (Figures 14d–14f and 15b). Figures 16e and 16f show the evolutions of these biases. Positive ozone bias of 0.35 ppmv was rapidly reduced toward 0.03 ppmv by the MLS assimilation. Then the temperature bias of about 0.2 K gradually decreased toward almost 0 K by about 16 days in EXP.MLS. Figure 17 shows the impacts of the MLS assimilation on the temperature bias represented by the difference of bias^f between EXP.MLS and EXP.O3-FREE. Both of these differences at 10 hPa for CCSR/NIES and at 50 hPa for MRI decreased on a similar time scale. Figure 18 shows scatter plots of the impact of

assimilation of MLS on the T bias, which is defined as the difference between EXP.O3-FREE and EXP.MLS, versus the bias in XO3. At 10 hPa (Figure 18a) in the CCSR/NIES model, substantial impacts on both T bias (-0.65 K) and XO3 bias (-1.45 ppmv) were found, whereas in the other two models, both of those were nearly zero. At 50 hPa, only MRI showed substantial impacts on both T and XO3 biases. This result suggests that a correction of T associated with ozone assimilation occurred with different models. However, the relaxation time at 50 hPa was longer (20 to 40 days) than that at 10 hPa (10 to 15 days). Therefore, some impacts other than direct radiative impacts may also be responsible for the reduction of the temperature bias in MRI.

[42] De Grandpré et al. [2009] also found that assimilation of ozone data improved the temperature forecast in the 3D-Var framework. They do not show any radiative impact

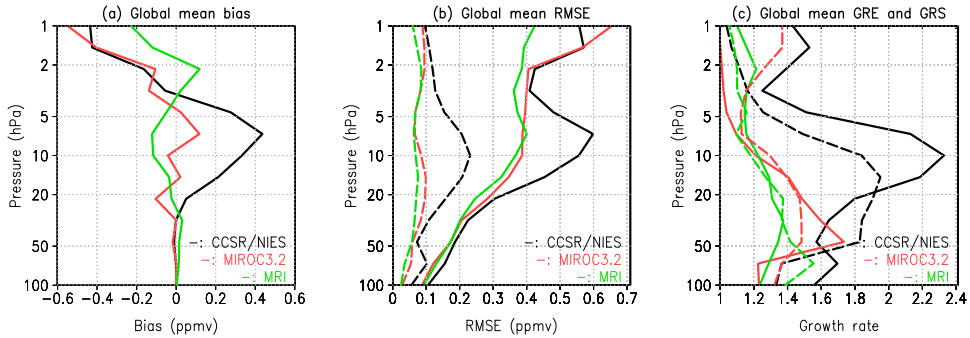


Figure 13. Vertical profiles of the spatiotemporal means (80°S – 80°N , 00 UTC 16 July to 18 UTC 31 August) of error statistics of XO3 in EXP.MLS for models CCSR/NIES, MRI, and MIROC. All errors were calculated against MLS ozone profiles. (a) Bias^f, (b) RMSE^f (solid line) and SPRD^f (dashed line), and (c) growth rate of the forecast/analysis error (GRE, solid line) and growth rate of the ensemble spread (GRS, dashed line).

of ozone assimilation below 10 hPa level. Our results suggest that a correction of the temperature bias associated with radiative impacts results from improvement of the ozone concentration. However, direct comparison of the effects of the temperature improvement by ozone assimilation between their study and the present study requires some caution because of differences in the assimilation methods, observation data, and the errors between our experiments

and theirs. For meteorological observation data, they used data from radiosondes, surface observations, aircraft winds, and so on, which, except over land in the NH, have lower observation densities than the reanalysis meteorological data used in this study (JCDAS). In addition, in our experiments, the magnitude of the observation error assumed for the JCDAS dataset was about half the magnitude of their observation error. Consequently, the meteorological field

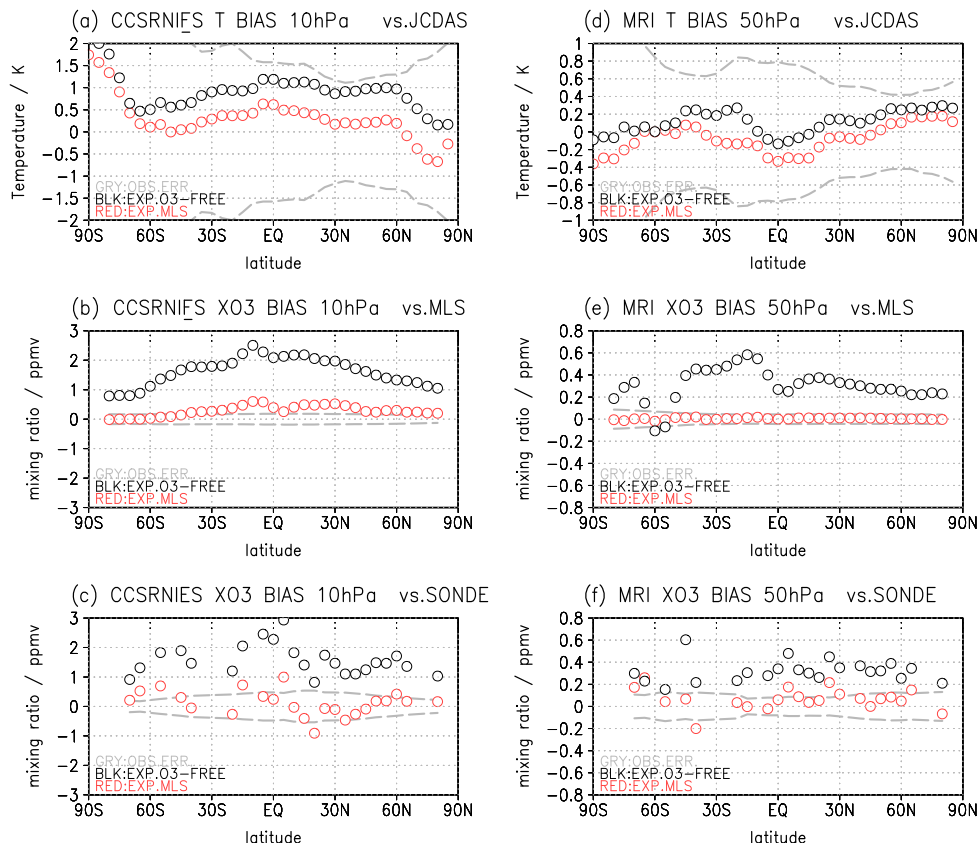


Figure 14. Zonal mean bias^f in (a and d) T and (b–f) XO3 at 10 hPa in the CCSR/NIES CCM (a–c) and at 50 hPa in the MRI CCM (d–f). The observational dataset used for the assimilation evaluation is shown at the top right of each panel. Black circles, EXP.O3-FREE biases; red circles, EXP.MLS biases; gray dashed lines, observation errors; and black triangles, EXP.O3-FREE biases in the MIROC3.2 CCM.

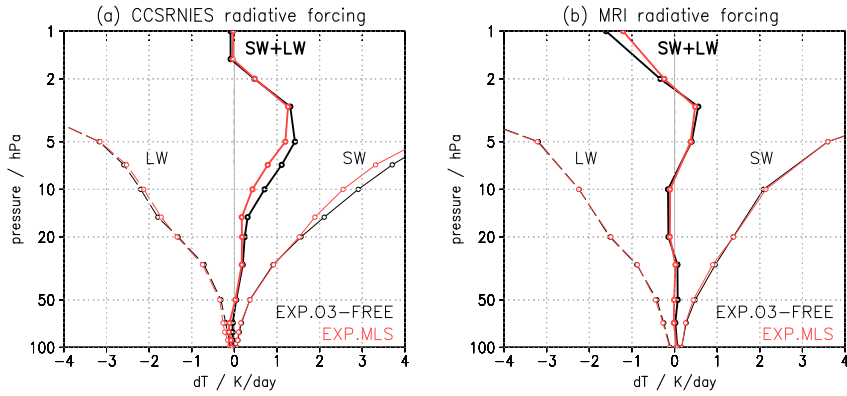


Figure 15. Vertical profiles of diabatic radiative heating averaged over the NH (30°N to 80°N) in (a) CCSR/NIES CCM and (b) MRI CCM. Thin solid lines, solar heating (SW); thin dashed lines, infrared radiative heating (LW); and thick solid lines, net radiative heating (SW + LW). Black lines, EXP.O3-FREE; red lines, EXP.MLS.

was more strongly constrained by observation data in our experiments than was the case in the experiments of *De Grandpré et al.* [2009]. If we had used raw observation data for the meteorological field data, the impact of ozone on temperature may have been accentuated more than the results presented here.

[43] The evolution of biases in temperature forecasts and the analysis of an experiment that considered the cross-covariance between XO₃ and meteorological fields are shown in Figure 16b by green lines. Negative temperature bias increased in the analysis compared with the forecast, an indication that the assimilation deteriorated in the temperature analysis. This deterioration was caused by the bias in ozone. LETKF reduced the ozone concentration versus the positive bias in ozone at 10 hPa (black and green lines in Figure 16a). Then because temperature and ozone are positively correlated at this altitude, LETKF reduced temperature simultaneously in spite of the negative bias in temperature. This inconsistency between temperature and ozone analyses that results from the model bias should be reduced by both model improvement and an assimilation technique such as bias correction [*Lin et al.*, 2008].

6.3. Model Dependency of the Assimilation Performance in the UTLS

[44] We diagnosed the growth of errors during the forecast step to examine model dependency in the UTLS. In the CCSR/NIES model, the GRE was larger than in the other models (Figure 19a). The ensemble spread was then larger than the observation errors (Figure 19b), indicating a limited reliability for the forecast, as compared to the observation. Figure 19c shows a scatter diagram of the increment against the innovation. The increment and innovation were obtained approximately, by bias^a minus bias^f , and the sign reversed bias^f (i.e., observation minus forecast, OmF), respectively. The increment of XO₃ then corresponded well to the innovation in the CCSR/NIES model (Figure 19c). This result indicates that SPRD^f captures the growing XO₃ errors well in the forecast step and, thus, the forecast errors are reduced according to the OmF in the analysis step. In contrast, the GRE and spread of CHASER were the smallest among the models. The slope of the increment against

innovation was also the smallest and resulted from a large reliance on the forecast of CHASER. The diagnoses of MIROC3.2 and MRI were intermediate. The results are almost the same at other pressure levels in the UTLS (146 and 215 hPa levels). Intermodel comparison results indicate that the reliability of the forecast is large (small) as the model-dependent error growth is small (large) in the UTLS.

[45] *Geer et al.* [2006] reported that in the UTLS region, errors in ozone analyses are strongly dependent on the model error due to transport. In this region, ozone behaves as a tracer because it has a much longer chemical life time than that in the middle and upper stratosphere. The reliability of ozone assimilation predictions should, therefore, be considerably affected by the performance of the tracer transport component of the models. Therefore, the different magnitudes of error growth shown in Figure 19a may reflect differences in the transport schemes. Only CCSR/NIES has a spectral advection (spectral transform and finite difference) scheme, with the other models having semi-Lagrange schemes (Table 1).

[46] Another factor to consider in the assimilation performance in the UTLS is the quality of data. As shown in Figure 10, the MLS assimilation successfully reduced biases until they were smaller than observational errors for all models in the UTLS. Comparisons against independent ozonesonde observations also indicated that the MLS assimilation performed well (Figure 9). Despite the different magnitudes of error growth, assimilation results (bias^f) were almost the same among models (Figure 10). This suggests that the MLS assimilation successfully reduced the model dependency on ozone analysis not only in the stratosphere but also in the UTLS.

6.4. Influence of Model Bias in the Troposphere

[47] As discussed in section 5.2, the assimilation of MLS ozone profiles (EXP.MLS) reduced errors in XO₃ in the stratosphere and thus improved the TO₃ performance in all of the models. In the troposphere, however, the assimilation should not be effective because of the lack of observations in the middle and lower troposphere and the large observation errors in the upper troposphere (Figure 9). This tropospheric

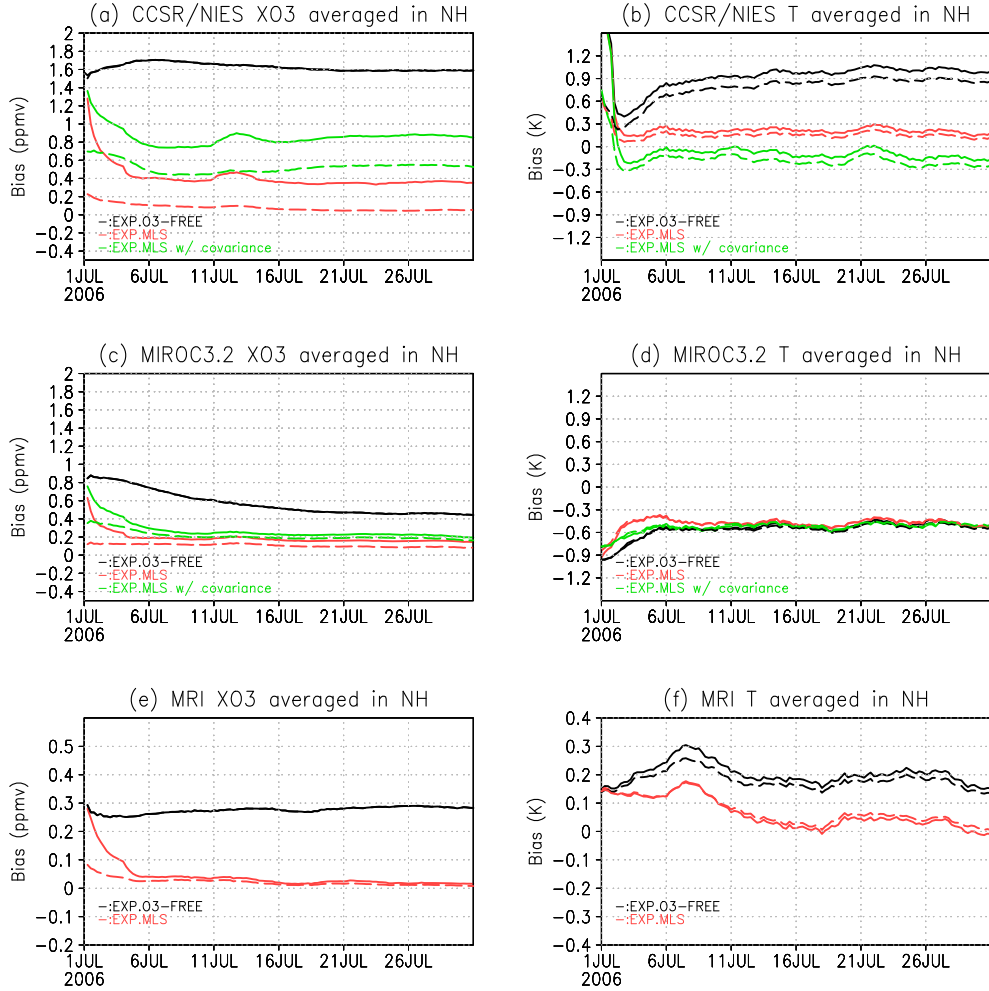


Figure 16. (a) Evolution of the NH averaged (30°N to 80°N) bias in ozone concentration at 10 hPa in the CCSR/NIES model. Solid and dashed lines denote bias of the forecast and analysis, respectively. Experiments corresponding to line colors are drawn in left-bottom corner of each panel. EXP.MLS with covariance (green lines) indicates results from the experiment identical to the EXP.MLS except for that the cross-covariance between the ozone and the meteorological fields are taken into consideration. (b) As in Figure 16a but for evolutions of bias in temperature. (c and d) For MIROC3.2 model. (e and f) As in Figure 16a and 16b but for 50 hPa and for MRI model.

bias in X03 might be a reason for the small remaining bias in TO3 when the MLS ozone was assimilated (Figures 12a and 12c). Moreover, the accuracy of X03 analyses with OMI-TOMS assimilation alone might be compromised by model bias in the troposphere. *Dethof and H  lm* [2004] reported that the vertical ozone concentration profile tends to deteriorate if only total ozone data are assimilated, because model bias may cause the background error covariance between TO3 and X03 to not be described correctly. Further, in most cases, ozone analyses by models lacking detailed tropospheric chemistry schemes cannot represent tropospheric ozone profiles well [*Geer et al.*, 2006]. In this study, CCSR/NIES and MIROC3.2 do not have detailed tropospheric chemistry schemes, but MRI and CHASER do. To assess the influence of the tropospheric bias on the assimilation results, we compared the relationship between the biases in TO3 and X03 among the models.

[48] NH stratospheric ozone profiles in CCSR/NIES and MIROC3.2 had large biases with TO3 assimilation

(Figures 9a and 9b, EXP.OMI, green lines), biases that were larger than, and thus magnified, the respective model biases (black lines). These models had large ozone concentration biases in the NH troposphere. In contrast, the stratospheric ozone concentrations in the MRI model did not show such large biases with TO3 assimilation because the bias of tropospheric ozone was small. In all models, tropospheric biases were smaller in the SH than in the NH. As a result, the biases in the stratospheric ozone concentration in the SH were successfully reduced by total ozone assimilation (not shown). Figure 20 shows the relationship between the RMSEs in tropospheric ozone and the RMSE difference in stratospheric ozone, where the RMSE difference is defined as the departure of the RMSE of EXP.MLS (X03 assimilation) or EXP.OMI (TO3 assimilation) from that of EXP.03-FREE. Positive (negative) values of the RMSE difference indicate that errors were increased (decreased) by the assimilation of MLS or OMI-TOMS observations. The correlation between tropospheric ozone RMSEs and the increase of stratospheric ozone errors was positive with

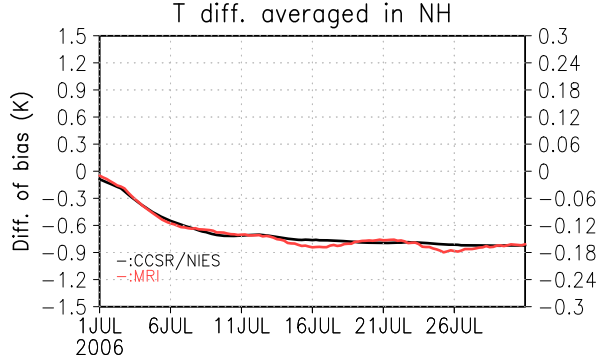


Figure 17. Evolution of difference of bias^f (EXP.MLS minus EXP.O3-FREE) at 10 hPa for CCSR/NIES (black line) and 50 hPa for MRI (red line). Vertical axis labeled at left (right) hand side indicates magnitudes of the difference for CCSR/NIES (MRI).

TO3 assimilation (green circles, $r=0.67$ with over 99.9% significance) but not with XO3 assimilation (red circles, $r=0.16$ with about 90% significance), a result that suggests that reducing the model bias in tropospheric ozone is important for better estimation of ozone profiles by the assimilation of the total ozone observations. Furthermore, assimilation of vertical ozone profiles in addition to total ozone is also effective in reducing the model biases at all altitudes, as shown by the EXP.FULL result (Figure 9, blue lines). Thus, the use of multiple observation datasets can also improve assimilation performance by reducing the effect of model bias.

7. Summary

[49] We compared the assimilation performance of ozone and meteorological fields of four chemical models using a LETKF assimilation system. Because the LETKF parameters were almost the same among the models, whereas the biases of each model were different, we were able to investigate the influence of the model biases on ozone data assimilation.

[50] Summary of the assimilation of MLS ozone profiles:

The model bias deteriorated the assimilation performance by amplifying the growth of errors and preventing the development of the ensemble spread. Both of these effects caused underestimation of the forecast error covariance. This was particularly the case in the middle stratosphere in the CCSR/NIES model (section 6.1).

An ozone bias causes a temperature bias through the radiation process. Therefore, in the middle stratosphere, reduction of the ozone bias by the assimilation of MLS ozone profiles led to a reduction of the temperature bias. Our multimodel study suggests that ozone assimilation is beneficial to the correction of the bias in temperature at least for the CCMs used in this study (section 6.2).

In the UTLS region, where ozone behaves like a tracer, no model dependence of the errors in ozone analyses was found, although difference of the growing errors in the forecast was found among the models. The high accuracy of MLS observations in this region and the good performance of the transport field in the CCMs may explain this result (section 6.3).

In the upper stratosphere and mesosphere, the MLS assimilation did not have a sufficient impact to correct the bias of the models. In this altitude range, the ozone spread rapidly converged to a photochemical equilibrium value. As a result, LETKF underestimated the forecast error of ozone because of the small ensemble spread relative to the observation error. To avoid underestimation of forecast error, inclusion of some other chemical species or chemical reaction rates into the data assimilation analysis may be necessary to perturb the chemical equilibrium state. Such an assimilation technique may be necessary in the upper stratosphere and mesosphere because at those altitudes, diurnal variation of ozone should be considered in calculating heating rates [Sassi et al., 2005] and in the estimation of the long-term ozone trends (Sakazaki et al., Diurnal ozone variations in the stratosphere revealed in observations from the Superconducting Submillimeter-Wave Limb-Emission Sounder (SMILES) onboard the International Space Station

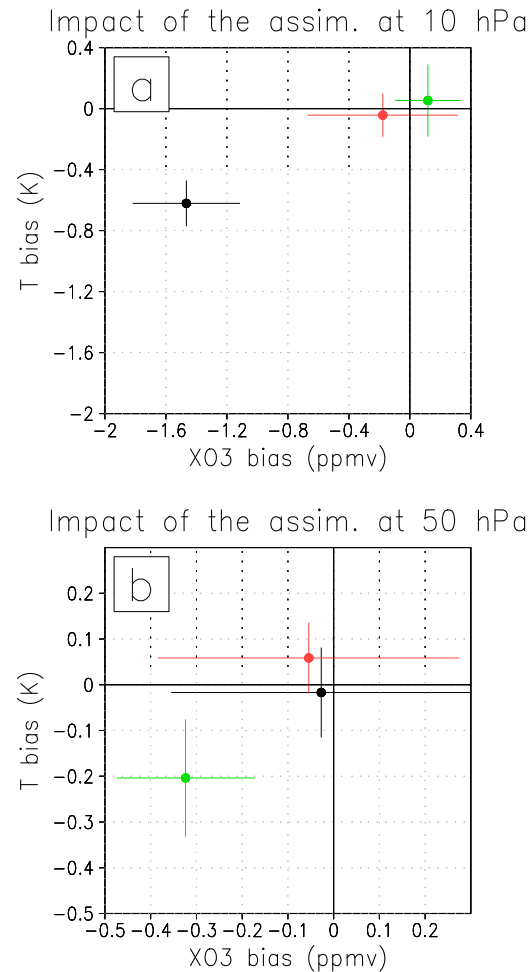


Figure 18. (a) Spatiotemporal mean and standard deviation of difference of bias^f (EXP.MLS minus EXP.FREE) in T against that in XO3 at 10 hPa. Horizontal and vertical axes are differences of bias in XO3 and T , respectively. Mean and standard deviation were computed by averaging from 30°N to 80°N and from 16 July to 31 August 2006. Dot denotes the mean, and bar denotes the standard deviation. Black, red, and green colors indicate CCSR/NIES, MIROC2.3, and MRI, respectively. (b) As in Figure 17a but for 50 hPa.

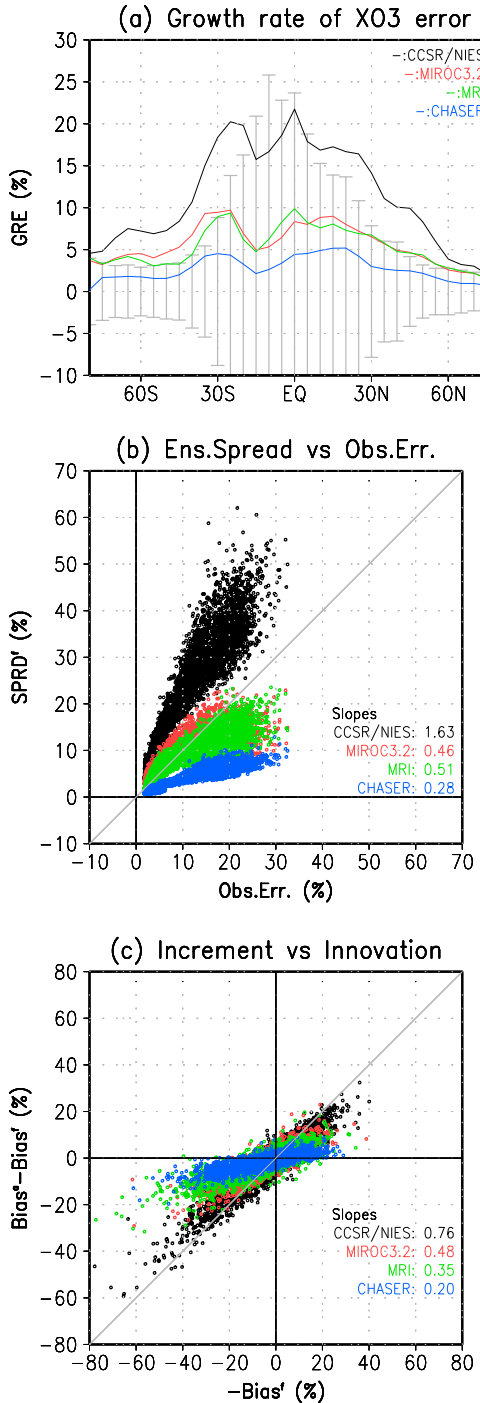


Figure 19. (a) GRE of X03 at 100 hPa averaged from 16 July to 31 August 2006. Models corresponding to the line colors are denoted at top right of the panel. Error bars denote the observation errors of MLS. The magnitudes are indicated by percentages (%) of the observation values of MLS. (b) Scatter diagram of ensemble spread of X03^f against observation errors of MLS between 80°S and 80°N from 16 July to 31 August 2006. Amplitude of the slope corresponding to each model is denoted at bottom right of the panel. (c) As in Figure 19b but for analysis increment against innovation. The increment is defined as bias^a minus bias^f. The innovation is defined as sign reversed value of bias^f.

(ISS), submitted to *Journal of Geophysical Research*, 2012] (section 5.2.1).

The error in total ozone was not substantially reduced by MLS ozone assimilation in the models with a tropospheric ozone error. This is evident in the CCSR/NIES and MIROC3.2 models, which showed a large bias in ozone in the troposphere (section 5.2.3).

Summary of the assimilation of OMI-TOMS total ozone:

Assimilation of OMI-TOMS total ozone data modified the modeled total ozone to values close to observations. In most cases, however, the ozone concentration profiles were deteriorated compared to the MLS ozone assimilation. This deterioration is evident in the CCSR/NIES and MIROC3.2 results, in which the bias in the tropospheric ozone concentration is large in the NH. Inaccurate specification of the background error covariance between X03 and TO3 is considered to be the primary cause of the deterioration. Applying vertical localization with an averaging kernel might be effective in improving the profiles when only total ozone data are used for assimilation (section 6.4).

Summary of the assimilation of MLS and OMI-TOMS:

Assimilation of both MLS and OMI-TOMS data greatly reduced biases in the ozone concentrations in both the stratosphere and the troposphere (section 5.2). Biases in total ozone were nearly zero, and the RMSE was smaller than the SCIAMACHY observation error in the NH and tropics. The combined use of MLS and OMI-TOMS data resulted in good assimilation performance for both the ozone profile and total ozone. In particular, the tropospheric bias, which remained with the assimilation of MLS alone, was effectively reduced by adding OMI-TOMS observations. As a result, the combined assimilation showed about 3% errors in the total ozone common to the three CCMs, whereas the MLS assimilation showed errors varying from 4 to 8% among models (section 5.3).

[51] Our results show that for the current models, the use of both stratospheric ozone profile data and total ozone data greatly improves the assimilation performance of global total ozone and the ozone profiles, regardless of the bias of the models. The results suggest that the use of multiple observations of ozone is effective in reducing the influence of the model bias and that the assimilation of ozone data improves the assimilation performance for temperature, particularly in the middle and upper stratosphere. However, it should be noted that the JCDAS reanalysis data were used as the observation data of meteorological fields in this study. The observation density and quality of reanalysis data substantially differ from those of real observations. As mentioned in section 6.2, we should be cautious in evaluating the impacts of ozone assimilation on the temperature analyses. In the future, LETKF ozone data assimilation of not only global satellite data but also a subset of local observational data, such as ozonesonde data, may allow more sophisticated ozone reanalysis by CCMs and CTMs. For better estimation of the ozone distributions, improved model skills for both local and global data are needed. Further, as demonstrated by Miyazaki *et al.* [2012b] for tropospheric

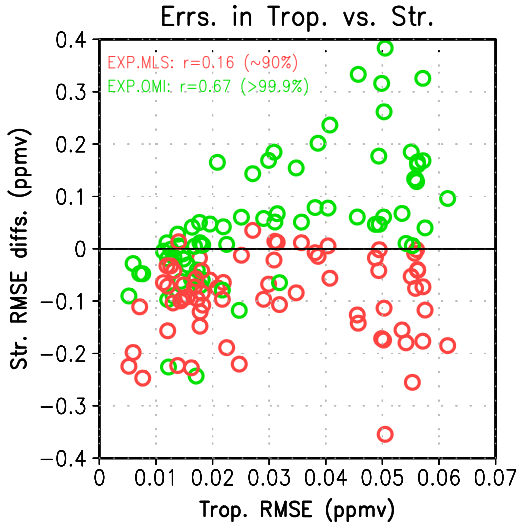


Figure 20. Scatter diagram of the tropospheric errors in XO3 versus the RMSE difference in XO3 in the stratosphere. The tropospheric error in XO3 is defined as the RMSE^f in XO3 of EXP.O3-FREE averaged between 700 and 300 hPa, and the RMSE difference in the stratosphere is defined as the departure of RMSE^f in XO3 of EXP.MLS (red) or EXP.OMI (green) from that of EXP.O3-FREE averaged between 100 and 30 hPa. Each circle corresponds to the error averaged over 5° latitude bins of three CCMs (CCSR/NIES, MIROC3.2, and MRI). Therefore, there are 108 circles (= 36 latitude bands × 3 models) for each experiment. Correlation coefficients and statistical significance corresponding to two experiments are shown at the top left of the figure.

chemistry, simultaneous assimilation of multiple chemical species that affect ozone might also be important for improvement of ozone assimilation. In the stratosphere HO_x, NO_x, and ClO_x as well as O_x control the ozone concentration. Certain skills in the assimilation of such transient reactive species and use of multiple satellite data involving these species will be required.

[52] **Acknowledgments.** The authors thank T. Miyoshi and M. Fujiwara for their advice on our analyses and T. Sekiyama for useful discussions. We would also like to thank the two anonymous reviewers and T. Milewski for their valuable comments. Computations were made on the NEC SX-8R computers at the Center for Global Environmental Research, National Institute for Environmental Studies (NIES). We also thank the MIROC model development group of the Atmospheric and Ocean Research Institute (University of Tokyo), Japan Agency for Marine-Earth Science and Technology (JAMSTEC), and NIES, and K. Sudo of Nagoya University. This study was supported by the Global Environment Research Fund of the Japanese Ministry of the Environment (A-0903). The GRENE Arctic Climate Change Research Project also supported a part of this study.

References

- Akiyoshi, H., L. B. Zhou, Y. Yamashita, K. Sakamoto, M. Yoshiki, T. Nagashima, M. Takahashi, J. Kurokawa, M. Takigawa, and T. Imamura (2009), A CCM simulation of the breakup of the Antarctic polar vortex in the years 1980–2004 under the CCMVal scenarios, *J. Geophys. Res.*, **114**, D03103, doi:10.1029/2007JD009261.
- Balis, D., M. Kroon, M. E. Koukouli, E. J. Brinksma, G. Labow, J. P. Veefkind, and R. D. McPeters (2007), Validation of Ozone Monitoring Instrument total ozone column measurements using Brewer and Dobson spectrophotometer ground-based observations, *J. Geophys. Res.*, **112**, D24S46, doi:10.1029/2007JD008796.
- Bhartia, P. K., C. G. Wellemeyer, S. L. Taylor, N. Nath, and A. Gopalan (2004), Solar backscatter ultraviolet (SBUV) version 8 profile algorithm, paper presented at Quadrennial Ozone Symposium, Int. Ozone Comm., Kos, Greece, 1–8 June.
- Bracher, A., L. N. Lamsal, M. Weber, K. Bramstedt, M. Coldewey-Egbers, and J. P. Burrows (2005), Global satellite validation of SCIAMACHY O₃ columns with GOME WFDOAS, *Atmos. Chem. Phys.*, **5**, 2357–2368, doi:10.5194/acp-5-2357-2005.
- Bracher, A., M. Weber, K. Bramstedt, L. N. Lamsal, and J. P. Burrows (2007), Total O₃ columns from SCIAMACHY OL3.0 to Sciamachy Weighting Function DOAS (WFDOAS), OMI-TOMS and GOME WFDOAS, in *Proceedings of the Third Workshop on the Atmospheric Chemistry Validation of Envisat (ACVE-3)*, 4–7 December 2006, ESRIN, Frascati, Italy (ESA SP-642, February 2007).
- Clark, H. L., M.-L. Cathala, H. Teyssèdre, J.-P. Cammas, and V.-H. Peuch (2007), Cross-tropopause fluxes of ozone using assimilation of MOZAIC observations in a global CTM, *Tellus*, **59B**, 39–49, doi:10.1111/j.1600-0889.2006.00243.x.
- Dee, D. P., et al. (2011), The ERA-Interim reanalysis: Configuration and performance of the data assimilation system, *Q. J. R. Meteorol. Soc.*, **137**, 553–597, doi:10.1002/qj.828.
- De Grandpré, J., R. Ménard, Y. J. Rochon, C. Charette, S. Chabriat, and A. Robichaud (2009), Radiative impact of ozone on temperature predictability in a coupled chemistry-dynamics data assimilation system, *Mon. Wea. Rev.*, **137**, 679–692, doi:10.1175/2008MWR2572.1.
- Dethof, A., and E. V. Hólm (2004), Ozone assimilation in the ERA-40 reanalysis project, *Q. J. R. Meteorol. Soc.*, **130**, 2851–2872, doi:10.1256/qj.03.196.
- Deushi, M., and K. Shibata (2011), Development of a meteorological research institute chemistry-climate model version 2 for the study of tropospheric and stratospheric chemistry, *Pap. Meteorol. Geophys.*, **62**, 1–46, doi:10.2467/mripapers.62.1.
- Elbern, H., J. Schwinger, and R. Botchorishvili (2010), Chemical state estimation for the middle atmosphere by four-dimensional variational data assimilation: System configuration, *J. Geophys. Res.*, **115**, D06302, doi:10.1029/2009JD011953.
- Eskes, H. J., P. F. J. van Velthoven, P. J. M. Valks, and H. M. Kelder (2003), Assimilation of GOME total ozone satellite observations in a three-dimensional tracer transport model, *Q. J. R. Meteorol. Soc.*, **129**, 590, 1663–1681, doi:10.1256/qj.02.14.
- Eyring, V., et al. (2006), Assessment of temperature, trace species, and ozone in chemistry-climate model simulations of the recent past, *J. Geophys. Res.*, **111**, D22308, doi:10.1029/2006JD007327.
- Froidevaux, L., et al. (2008), Validation of Aura Microwave Limb Sounder HCl measurements, *J. Geophys. Res.*, **113**, D15S25, doi:10.1029/2007JD009025.
- Geer, A. J., et al. (2006), The ASSET intercomparison ozone analyses: Method and first results, *Atmos. Chem. Phys.*, **6**, 5445–5474, doi:10.5194/acp-6-5445-2006.
- Gettelman, A., et al. (2010), Multimodel assessment of the upper troposphere and lower stratosphere: Tropics and global trends, *J. Geophys. Res.*, **115**, D00M08, doi:10.1029/2009JD013638.
- Hilsenrath, E., B. R. Bojkov, G. Labow, and A. Bracher (2004), SCIAMACHY column ozone validation, in *Proceedings of the Second Workshop on the Atmospheric Chemistry Validation of ENVISAT (ACVE-2)*, ESA-ESRIN, Frascati, Italy, 3–7 May 2004 (ESA SP-562, August 2004) ESC01EH.
- Hunt, B. R., E. J. Kostelich, and I. Szunyogh (2007), Efficient data assimilation for spatiotemporal chaos: A local ensemble transform Kalman filter, *Physica D*, **230**, 112–126, doi:10.1016/j.physd.2006.11.008.
- Kalman, R. E. (1960), A new approach to linear filtering and prediction problems, *Trans. ASME Ser. D. J. Basic Eng.*, **82**, 35–45.
- Kalnay, E., (2003), *Atmospheric Modeling, Data Assimilation and Predictability*, 341 pp., Cambridge University Press, New York.
- Kalnay, E., et al. (1996), The NCEP/NCAR 40-year reanalysis project, *Bull. Am. Meteorol. Soc.*, **77**, 437–471.
- Kalnay, E., H. Li, T. Miyoshi, S. C. Yang, and J. Ballabrera-Poy (2007), 4-D-Var or ensemble Kalman filter?, *Tellus, Ser. A*, **59**, 758–773, doi:10.1175/BAMS-83-11-1631.
- Kanamitsu, M., W. Ebisuzaki, J. Woollen, S.-K. Yang, J. J. Hnilo, M. Fiorino, and G. L. Potter (2002), NCEP/DOE AMIP-II reanalysis (R-2), *Bull. Am. Meteorol. Soc.*, **83**, 1631–1643, doi:10.1175/BAMS-83-11-1631.
- Kiesewetter, G., B.-M. Sinnhuber, M. Vountas, M. Weber, and J. P. Burrows (2010), A long-term stratospheric ozone data set from assimilation of satellite observations: High-latitude ozone anomalies, *J. Geophys. Res.*, **115**, D10307, doi:10.1029/2009JD013362.
- Lahoz, W. A., R. Brugge, D. R. Jackson, S. Migliorini, R. Swinbank, D. Lary, and A. Lee (2005), An observing system simulation experiment to evaluate the scientific merit of wind and ozone measurements from the future swift instrument, *Q. J. R. Meteorol. Soc.*, **131**, 503–523, doi:10.1256/qj.03.109.

- Levelt, P. F., G. H. J. van den Oord, M. R. Dobber, A. Malkki, H. Visser, J. de Vries, P. Stammes, J. O. V. Lundell, and H. Saari (2006), The ozone monitoring instrument, *IEEE Trans. Geosci. Remote Sens.*, **44**, 1093–1101, doi:10.1109/TGRS.2006.872333.
- Li, H., E. Kalnay, and T. Miyoshi (2009a), Simultaneous estimation of covariance inflation and observation errors within ensemble Kalman filter, *Q. J. R. Meteorol. Soc.*, **135**, 523–533, doi:10.1002/qj.371.
- Li, H., E. Kalnay, T. Miyoshi, and C. M. Danforth (2009b), Accounting for model errors in ensemble data assimilation, *Mon. Wea. Rev.*, **137**, 3407–3419, doi:10.1175/2009MWR2766.1.
- Lin, C., J. Zhu, and Z. Wang (2008), Model bias correction for dust storm forecast using ensemble Kalman filter, *J. Geophys. Res.*, **113**, D14306, doi:10.1029/2007JD009498.
- Liu, J., I. Y. Fung, E. Kalnay, J.-S. Kang, E. T. Olsen, and L. Chen (2012), Simultaneous assimilation of AIRS Xco₂ and meteorological observations in a carbon climate model with an Ensemble Kalman Filter, *J. Geophys. Res.*, **117**, D05309, doi:10.1029/2011JD016642.
- Livesey, N. J., et al. (2008), Validation of Aura Microwave Limb Sounder O₃ and CO observations in the upper troposphere and lower stratosphere, *J. Geophys. Res.*, **113**, D15S02, doi:10.1029/2007JD008805.
- Massart, S., C. Clerbaux, D. Cariolle, A. Piacentini, S. Turquety, and J. Hadji-Lazaro (2009), First steps towards the assimilation of IASI ozone data into the MOCAGE-PALM system, *Atmos. Chem. Phys.*, **9**, 5073–5091, doi:10.5194/acp-9-5073-2009.
- McCarty, W., G. Jedlovec, and T. L. Miller (2009), Impact of the assimilation of Atmospheric Infrared Sounder radiance measurements on short-term weather forecasts, *J. Geophys. Res.*, **114**, D18122, doi:10.1029/2008JD011626.
- McNally, A. P., P. D. Watts, J. A. Smith, R. Engelen, G. A. Kelly, J. N. Thépaut, and M. Matricardi (2006), The assimilation of AIRS radiance data at ECMWF, *Q. J. R. Meteorol. Soc.*, **132**, 935–957, doi:10.1256/qj.04.171.
- McPeters, R., M. Kroon, G. Labow, E. Brinksma, D. Balis, I. Petropavlovskikh, J. P. Veefkind, P. K. Bhartia, and P. F. Levelt (2008), Validation of the Aura Ozone Monitoring Instrument total column ozone product, *J. Geophys. Res.*, **113**, D15S14, doi:10.1029/2007JD008802.
- Milewski, T., and M. S. Bourqui (2011), Assimilation of stratospheric temperature and ozone with an Ensemble Kalman Filter in a chemistry-climate model, *Mon. Wea. Rev.*, **139**, 3389–3404, doi:10.1175/2011MWR3540.1.
- Miyazaki, K. (2009), Performance of a local ensemble transform Kalman filter for the analysis of atmospheric circulation and distribution of long-lived tracers under idealized conditions, *J. Geophys. Res.*, **114**, D19304, doi:10.1029/2009JD011892.
- Miyazaki, K., H. J. Eskes, and K. Sudo (2012a), Global NO_x emission estimates derived from an assimilation of OMI tropospheric NO₂ columns, *Atmos. Chem. Phys.*, **12**, 2263–2288, doi:10.5194/acp-12-2263-2012.
- Miyazaki, K., H. J. Eskes, K. Sudo, M. Takigawa, M. van Weele, and K. F. Boersma (2012b), Simultaneous assimilation of satellite NO₂, O₃, CO, HNO₃ data for the analysis of tropospheric chemical composition and emissions, *Atmos. Chem. Phys.*, **12**, 9545–9579, doi:10.5194/acp-12-9545-2012.
- Miyoshi, T., and S. Yamane, (2007), Local ensemble transform Kalman filtering with an AGCM at a T159/L48 resolution, *Mon. Wea. Rev.*, **135**, 3841–3861, doi:10.1175/2007MWR1873.1.
- Onogi, K., et al. (2007), The JRA-25 reanalysis, *J. Meteor. Soc. Japan*, **85**, 369–432, doi:10.2151/jmsj.85.369.
- Pajot, B., S. Massart, D. Cariolle, A. Piacentini, O. Pannekoucke, W. A. Lahoz, C. Clerbaux, P. F. Coheur, and D. Hurtmans (2011), High resolution assimilation of IASI ozone data with a global CTM, *Atmos. Chem. Phys. Discuss.*, **11**, 29,357–29,406, doi:10.5194/acpd-11-29357-2011.
- Sassi, F., B. A. Boville, D. Kinissou, and R. R. Garcia (2005), The effect of interactive ozone chemistry on simulations of the middle atmosphere, *Geophys. Res. Lett.*, **32**, L07811, doi:10.1029/2004GL022131.
- Sekiya, T. T., M. Deushi, and T. Miyoshi (2011), Operation-oriented ensemble data assimilation of total column ozone, *SOIA*, **7**, 41–44, doi:10.2151/sola.2011-011.
- Semane, N., V.-H. Peuch, S. Pradier, G. Desroziers, L. El Amaoui, P. Brousseau, S. Massart, B. Chapnik, and A. Peuch (2009), On the extraction of wind information from the assimilation of ozone profiles in Météo-France 4-D-Var operational NWP suite, *Atmos. Chem. Phys.*, **9**, 4855–4867, doi:10.5194/acp-9-4855-2009.
- Shibata, K., and M. Deushi (2008), Long-term variations and trends in the simulation of the middle atmosphere 1980–2004 by the chemistry-climate model of the Meteorological Research Institute, *Ann. Geophys.*, **26**, 1299–1326, doi:10.5194/angeo-26-1299-2008.
- Smit, H. G. J., et al. (1998), The 1996 WMO International intercomparison of ozonesondes under quasi flight conditions in the environmental simulation chamber at Jülich, in *Proceedings of the XVIII Quadrennial Ozone Symposium*, edited by R. Bojkov, and G. Visconti, 971–974, L’Aquila, Italy, September 1996.
- Smit, H. G. J., et al. (2007), Assessment of the performance of ECC-ozonesondes under quasi-flight conditions in the environmental simulation chamber: Insights from the Jülich Ozone Sonde Intercomparison Experiment (JOSIE), *J. Geophys. Res.*, **112**, D19306, doi:10.1029/2006JD007308.
- Son, S.-W., et al. (2010), Impact of stratospheric ozone on Southern Hemisphere circulation change: A multimodel assessment, *J. Geophys. Res.*, **115**, D00M07, doi:10.1029/2010JD014271.
- SPARC CCMVal (2010), SPARC CCMVal report on the evaluation of chemistry-climate models, edited by V. Eyring, T. G. Shepherd, and D. W. Waugh, Tech. Rep. SPARC Report No. 5, WCRP-132, WMO/TD-No. 1526, <http://www.sparc-climate.org/>.
- Sudo, K., M. Takahashi, J. Kurokawa, and H. Akimoto (2002a), CHASER: A global chemical model of the troposphere. 1. Model description, *J. Geophys. Res.*, **107**(D17) 4339, doi:10.1029/2001JD001113.
- Sudo, K., M. Takahashi, and H. Akimoto (2002b), CHASER: A global chemical model of the troposphere. 2. Model results and evaluation, *J. Geophys. Res.*, **107**(D21), 4586, doi:10.1029/2001JD001114.
- Thompson, D. W. J., J. C. Furtado, and T. G. Shepherd (2006), On the tropospheric response to anomalous stratospheric wave drag and radiative heating, *J. Atmos. Sci.*, **63**, 2616–2629, doi:10.1175/JAS3771.1.
- Uppala, S. M., et al. (2005), The ERA-40 re-analysis, *Q. J. R. Meteorol. Soc.*, **131**, 2961–3012, doi:10.1256/qj.04.176.
- Waters, J. W., et al. (2006), The Earth observing system microwave limb sounder (EOS MLS) on the aura Satellite, *IEEE Trans. Geosci. Remote Sens.*, **44**, 1075–1092, doi:10.1109/TGRS.2006.873771.